Sheath folds in simple shear:
An analytical and experimental study

Jacqueline E. Reber

Thesis submitted for the degree of
Philosophiae Doctor

Department of Geosciences
Faculty of Mathematics and Natural Sciences
University of Oslo, Norway

August, 2012

Series of dissertations submitted to the
Faculty of Mathematics and Natural Sciences, University of Oslo
No. 1250

ISSN 1501-7710

Cover: Inger Sandved Anfinsen.
Printed in Norway: AIT Oslo AS.

Produced in co-operation with Akademika publishing.
The thesis is produced by Akademika publishing merely in connection with the thesis defence. Kindly direct all inquiries regarding the thesis to the copyright holder or the unit which grants the doctorate.

Principal supervisor:
Dr. Daniel W. Schmid

Subsidiary supervisors:
Dr. Marcin Dabrowski
Dr. Olivier Galland

A great pleasure in life is doing what people say you cannot do.

W. Bagehot (1826-77)

Contents

Acknowledgements

Well, a couple of years back I couldn't imagine that I will ever be at this point where I will have to write the acknowledgements to my PhD thesis. Becoming a geologist was for a long time not something that occurred to me, but fortunately, after some detours, I discovered my love for stones and structures. Here, I would like to thank all of those people who believed in me.

Thank you, Dani, for being my main supervisor. You provided the perfect supervision for me where you let me discover myself what I'm interested in, even though it diverged quite a bit from the original plan. Thanks for all the good conversations, the talking in Schwiizerdütsch, and your straightforward way of being.

Thank you, Marcin, for supervising my analytical studies and giving me helpful advice whenever I really got stuck.

Thank you, Olivier, for being willing to join the supervisor team and introducing me to the laboratory techniques. It was great fun working with you in the lab.

Thank you, Torgeir, for supervising the first part of my PhD and taking me to the field in Western Norway.

I would like to say a special thank you to Stefan Schmalholz and Marcel Frehner. Stefan, you where the reason I started being interested in quantitative structural geology and you encouraged me to start a PhD. Thanks for listening to all my doubts till late at night and for providing the necessary encouragements. Marcel, your good example was always very inspiring.

Also special thanks go to Karen. Thank you for being a good friend and mentor.

Thank you, Marta and Maya. You were fun office mates and the girls office definitely rocked.

Thank you, Inge and Kirsten. Talking science with you was always very inspiring and helped me structure my thoughts. You also broadened my horizon outside of science; our weekly to daily exchange of music was entertaining and educating.

Thank you, Alban, Galen, Sonja, Camilla, Anja, François, Larissa for funny lunches, thank you, Stephanie and Conny for swimming and other physically painful sports, thank you, German mafia aka Andreas, Olli, and Jörn for grilling and other nice social events, thank you, Douwe for helpful writing comments and good concert suggestions. Thank you to all of you at PGP you made my last three years interesting and unforgettable.

Thank you, Ingrid, Nina, Maarten, and Karin for being my friends inside and outside of PGP.

Thank you to my friends back home, Andrea, Adi, Sarah, Eli, and Klara for being there for me whenever I needed you.

Thank you to all the PhDs and Students in Rennes who welcomed me with open arms, lots of beer, and petit' velos. A special thank you to Melanie, Melody, Jean-Jacques, Lorraine, Ceb, Stephen, Eline, Justine, and Silvia.

Thank you to my family and extended family for support of all kind.

The biggest thank you of all, however, goes to Chrigi. Without you, I wouldn't have been able to do any of this. You are the stable point and safe haven in my life.

Preface

Sheath folds are peculiar looking folds with a complex three-dimensional shape resembling a cone. These folds are often associated with shear zones and they are considered as a potential source of information for a kinematic and mechanical interpretation of shear zones. Even though sheath folds have been used to infer strain magnitude, bulk strain, and shear sense in shear zones, little is known about the relation between the cause of the fold, the amount of strain, the bulk strain, and the resulting shape of the fold. The aim of this thesis is to investigate the formation and evolution of sheath folds in simple shear and obtain a better understanding of how the initial configurations, leading to the fold, manifest themselves in the resulting fold shape, and ultimately, how reliable the information obtained from sheath folds is. With a combined analytical and experimental approach, a new formation mechanism for sheath fold formation is tested and a wide parameter space investigated.

1. Introduction

Folds. Their aesthetics and the fact that something as hard as rock can be deformed, bent, and folded has fascinated, interested, and riddled scientists for many years (Steno, 1669). Studies of folds started with sketches (Scheuchzer, 1718). Over time, several scientifically reasoned explanations for the formation of folds were presented. Hutton (1788) suggested that magma flowed from the middle of the earth towards the crust leading to its deformation and resulting ultimately in the formation of mountains. De Saussure (1796) remarked that a vertical uplift was not enough to explain steeply dipping fold limbs. He suggested, therefore, that an additional horizontal force had to be involved. The idea of a shrinking earth interior causing the crust to deform and mountains to form by folding (de Beaumont, 1852) incorporated the idea of a vertical and horizontal movement. By studying the stratigraphy (Hall, 1843) patterns of reoccurring lithologies could be attributed to folding. With the establishment and acceptance of the theory of continental drift, folds started to be recognized as the result of moving, colliding, and separating crustal plates (Wegener, 1929). The fact, however, that something as solid as a rock can be deformed as easily as modeling clay might be hard to grasp when one does not consider the time scale of geological processes and the extreme temperatures and pressures involved in the deformation. Under geological time scales, rocks behave like viscous fluids (Ranalli, 1995), which means that they deform permanently following specific flow-laws when subjected to stress. This realization made it possible to study folds by means of models, scaling their physical parameters such as pressure, temperature, time, stress, and strain (e.g., Willis, 1894).

Over 300 years of studying folds first in the field then with analogue (e.g., Hall, 1815; Biot et al., 1961; Ramberg, 1963; Ghosh and Ramberg, 1968), analytical (e.g., Biot, 1957, 1961; Fletcher, 1974, 1977; Smith, 1977, 1979), and numerical (e.g., Chapple, 1968; Dieterich, 1969; Parrish, 1973; Frehner and Schmalholz, 2006;

Schmid et al., 2008) models led to an abundant collection of names and classifications (e.g., Harding, 1973; Hudleston and Treagus, 2010; Adamuszek et al., 2011). The study area of folds in structural geology broadened over time and folds in different settings caused by different processes were described and studied.

This thesis is dedicated to the study of one special type of folds in a specific deformational regime: Sheath folds in simple shear.

1.1. What is a sheath fold?

The term sheath fold originates from the resemblance of the fold to a sheath. In the early literature they have been described using different names such as ‘saddle folds’ (Quirke and Lacy, 1941), ‘closed folds’ (Balk, 1953), ‘cone structures’ (Ramsay, 1958), ‘paraboidal folding’ (Carey, 1962), ‘eye folds’ (Nicholson, 1963), or ‘tubular folds’ (Hansen, 1971). The term sheath fold seems to appear for the first time in a geological survey paper of Canada in 1935 and since Carreras et al. (1977) the term is firmly established. Note that the term sheath fold is purely descriptive and is not associated with any formation mechanism.

Sheath folds have been described in the literature in many different ways. Ramsay and Huber (1987) described them as folds in which the hinge line orientation changes more than 90°. Ghosh et al. (1999) added that the folds are planar, *i.e.* they show a planar axial surface. Marques et al. (2008) completed this definition by adding that the hinge must be curved within the axial surface. Morales et al. (2011) pointed out that the folds show a hinge line sub-parallel to the local stretching lineation, while Crispini and Capponi (1997) simply described sheath folds as highly non-cylindrical folds. These examples make it already apparent that it is not easy to describe sheath folds in an unambiguous way. The main problem is that sheath folds are three-dimensional structures with a high complexity. Figure 1 shows a sketch of a sheath fold. To capture the three-dimensional aspect of the fold it can be described as cone shaped, where the tip or apex of the cone is rounded. The cone can be stretched and flattened to exhibit a more elliptical base area (Figure 2). The base area in a sheath fold contains the closed contours and builds the characteristic eye-pattern. Skjernaa (1989) established the difference between sheath folds and tubular folds based on the opening angle of the cone. Sheath folds have an opening angle between

90° and 20° and tubular folds have an opening angle of less than 20°. Alsop and Holdsworth (2004b) coined the term tongue folds for folds that were clearly non-cylindrical but did not classify as sheath folds *senso stricto, i.e.* showing an opening angle between 90° and 160°.

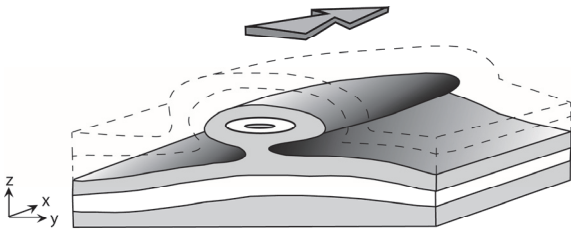

Figure 1: Sketch of a sheath fold produced by shearing. The gray arrow indicates the shear direction.

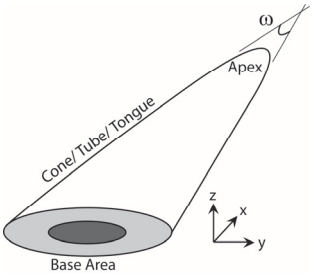

Figure 2: Sketch illustrating the different terms used for the description of highly non-cylindrical folds. ω: Cone opening angle.

In some cases, sheath folds can be observed in the field in three-dimensions (Figure 3a; Carreras et al., 1977; Quinquis et al., 1978; Alsop and Carreras, 2007; Kuiper et al., 2007; Srivastava, 2011). Most of the time, however, only cross-sections can be found (e.g., Minnigh, 1979; Henderson, 1981; Skjernaa, 1989; Goscombe, 1991; Ghosh et al., 1999; Alsop and Holdsworth, 2006; Srivastava, 2011). Figure 3 shows examples of sheath folds, three-dimensional outcrops (a and h) and cross-sections (b, c, d, e, f, and g). Cross-sections cut perpendicular to the elongation direction of the fold show closed elliptical shapes nested in each other forming eye-like structures. Using a Cartesian coordinate system the consensus is that the length of the tube or tongue is along the x-axis (Alsop and Holdsworth, 2006). Cross-

sections displaying closed contours are cut perpendicular to the x-axis in the y-z plane.

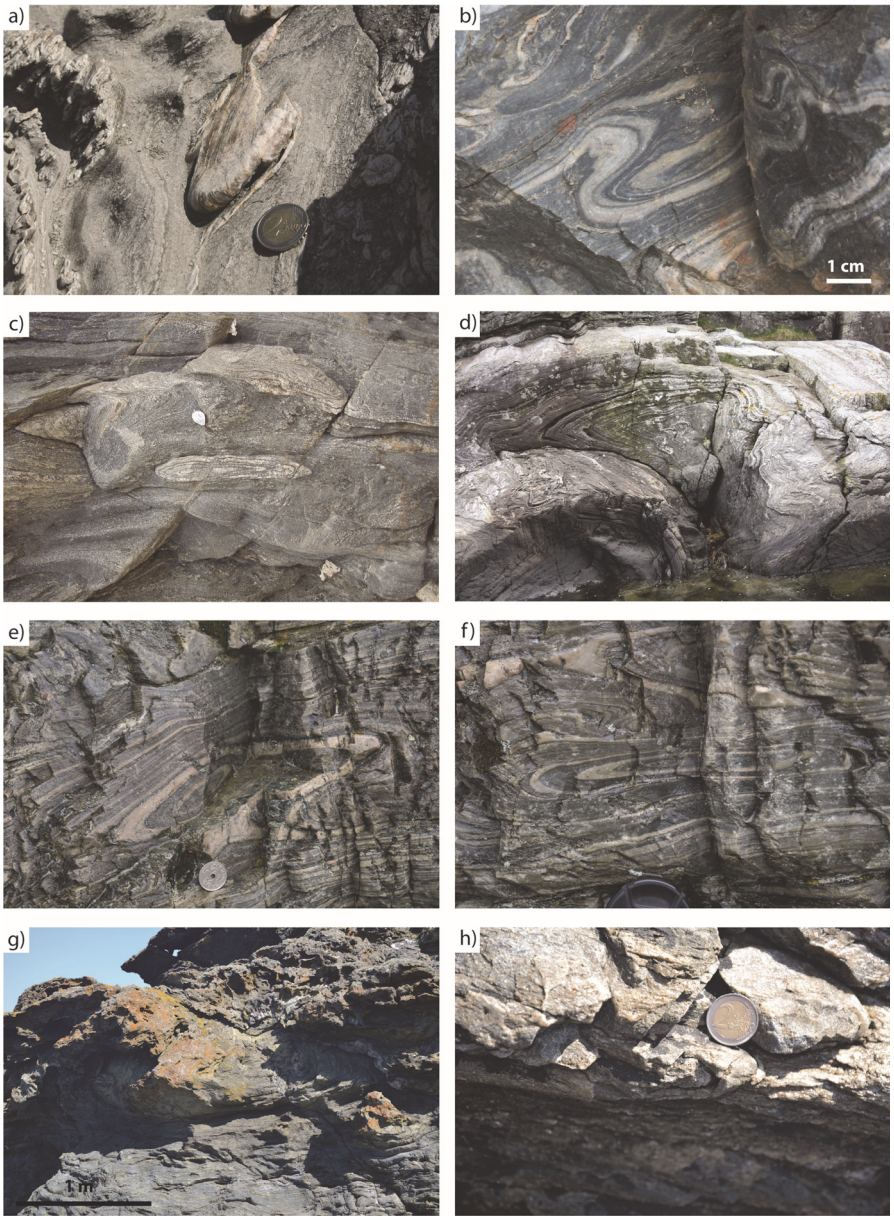

Figure 3: Photographs of outcrop scale sheath folds. a), b), and c) Cap de Creus, Spain, d) Sauesundøyane, Norway, e) and f) Oppdal, Norway, g) and h) Ile de Groix, France.

1.2. Occurrence of sheath folds

Sheath folds have been described in many different rock-types and materials such as metamorphic rocks (e.g., Carreras et al., 1977; Minnigh, 1979; Philippon et al., 2009; Srivastava, 2011), soft sediments (Hibbard and Karig, 1987; George, 1990; McClelland et al., 2011), glaciotectonic sediments (e.g., Thomas and Summers, 1984; Kluiving et al., 1991; Moller, 2006), pseudotachylites (Berlenbach and Roering, 1992), salt (e.g., Kupfer, 1976; Talbot and Jackson, 1987; Alsop et al., 2007), and ignimbrites (Branney et al., 2004). The size of the sheath fold can vary considerably. They range from submillimeters (in pseudotachylites, Berlenbach and Roering, 1992) to several kilometers (in metamorphic nappes, e.g., Lacassin and Mattauer, 1985; Searle and Alsop, 2007; Bonamici et al., 2011) in size. It is not established how common sheath folds are in nature. Alsop and Holdsworth (2006) were able to measure 1425 cross-sections of sheath folds in metamorphic rocks for their study on sheath folds as discriminators of bulk strain type, showing that sheath folds can be found all over the world. The term sheath fold appears in over 170 papers published over the last 30 years.

1.3. How do sheath folds form?

The following section discusses the formation of sheath folds in pure-, general-, and simple-shear. Pure shear can be described as a homogeneous, non-rotational deformation where material lines parallel to the principal axes of strain do not rotate (Twiss and Moores, 2007). In pure shear, a cube with edges parallel to the coordinate axes gets distorted into a brick-shaped body. In simple shear, the deformation involves besides a non-zero strain component also a non-zero rotational component (Means, 1976). An example of simple shear is the shearing of a deck of cards, laying flat on a table. In general shear an additional pure shear component is added to the simple shear deformation. As the term sheath fold is purely descriptive, all the mechanisms that will be discussed in the following paragraphs can potentially lead to their formation. Additional structural observations, such as the lineation on the fold or additional strain type indicators are needed to determine under which bulk strain type the sheath fold developed.

1.3.1. Pure shear

Some studies suggest that sheath folds can form in a pure shear bulk strain type (Ghosh and Sengupta, 1984; Ez, 2000; Alsop and Holdsworth, 2004a, 2006; Carreras et al., 2005; Mandal et al., 2009). Their formation is proposed to be similar to the development of dome structures (e.g., Ramsay and Huber, 1987) where equal shortening from two perpendicular directions is needed. The only difference between a sheath fold and a dome structure, both generated through the same type of deformation, is that the opening angle of a sheath fold has to be smaller than 90°, so they classify as sheath folds. A sheath fold has a smaller opening angle and steeper flanks than a dome structure, otherwise the formation mechanism is essentially the same. In other words, as long as the angle requirement by the classification of Ramsay and Huber (1987) is fulfilled, sheath folds in pure shear can also be described as the result of fold interference (Ramsay, 1967; Grasemann et al., 2004). Nicolas and Boudier (1975) observed sheath folds in peridotites, which they interpreted as the result of a constrained flow in an asthenospheric intrusion. Ez (2000) argued that constriction or flattening, which are both non-rotational deformations but show length changes in two directions, are the dominant formation mechanism for the formation of sheath folds. Fletcher (1991) and Schmid et al. (2008), however, showed that dome and basin structures and, therefore, sheath folds develop only under special conditions where there is exactly the same amount of shortening in both perpendicular directions. Mandal et al. (2009) presented a numerical study on the development of sheath folds from an initial irregularity in the hinge line of a cylindrical fold in pure shear. The study took a homogeneous matrix as well as a mechanically layered matrix into account. They concluded that sheath folds only develop in a matrix with a viscosity ratio over 10 when the initial perturbation is significant. For a lower viscosity ratio, the initial perturbation can be smaller and sheath folds still develop.

1.3.2. General shear

The shear deformation resulting from adding a simple shear component to pure shear is termed general shear. Alsop and Holdsworth (2006) showed several examples of sheath folds that developed in general shear. Even though not many

sheath folds are described for a general shear environment in the literature, it is rather common to have general shear conditions in nature (e.g., Holdsworth and Roberts, 1984; Stauffer and Lewry, 1993; 2002; Ghosh et al., 1999; Carosi and Oggiano), Also shear zones which are described as simple shear dominated (e.g., Minnigh, 1979; Fossen and Rykkelid, 1990; Harms et al., 2004) do not exclude a pure shear component.

Jiang and Williams (1999) examined the rotation of folds and the development of sheath folds in general three-dimensional zonal deformation. They show under which flow conditions sheath folds can develop from pre-existing perturbations. Kuiper et al. (2007) investigated the impact of a pure shear component on the orientation of the x-axis of sheath folds in high strain zones by means of numerical modeling. They conclude that well developed sheath folds are unreliable indicators for the shear direction.

1.3.3. Simple shear

In contrast to Ez's (2000) statement, simple shear is generally thought to be the most important bulk strain type for the formation of sheath folds (e.g., Fossen, 2010; Van der Pluijm and Marshak, 2004). The general idea of forming sheath folds in simple shear is by perturbation of the simple shear flow. In the literature, two different triggers were suggested: the amplification of a pre-existing perturbation and a rigid inclusion. The papers presented in this thesis show the possibility of yet another potential formation mechanism: the flow perturbation around a weak inclusion.

In nature it is, in many cases, impossible to determine the cause of the sheath fold formation. This can be either because the precursor might be overprinted by the strain or because the resulting fold may be separated from the perturbing structure in the shear zone. An additional difficulty is that many sheath folds are only partially outcropping. It is thus difficult to unambiguously determine the cause for most natural sheath folds.

1.3.3.1. Passive amplification

The sheath fold formation due to passive amplification of an initial perturbation has dominated the thinking of how sheath folds form for over a quarter

of a century. This idea combined with the necessity for a high finite and inhomogeneous strain as cause for sheath folds can be found in numerous structural geology textbooks (Davis and Reynolds, 1984; Van der Pluijm and Marshak, 2004; Pederson and Dehler, 2005; Fossen, 2010).

Cobbold and Quinquis (1980) conducted experiments using silicone and plasticine as rock analogues to test if a pre-existing perturbation in a layer can lead to the formation of sheath folds in simple shear (Figure 4a). They performed three different experiments with a shear strain of $\gamma = 15$. In the first model, they deformed a homogeneous matrix with a marker layer to visualize the deformation. The marker layer was perturbed, *i.e.* it had a small dent in its center, before the model was sheared. This perturbation was initially symmetric but with increasing deformation became deformed, stretched, and strongly asymmetric resulting in the formation of a sheath fold. The fold developed purely passively and its shape depended on the initial shape of the deflection. In this case, the simple shear flow did not get perturbed, as the entire matrix was homogeneous. In a second experiment, they tested the impact of a rigid and corrugated basement on the overlaying, weaker layer (Figure 4b). The model was built of two layers, one representing the stiff basement and the other the overlying, less viscous layer. The overlaying layer had passive marker layers for the visualization of the deformation. The corrugation of the basement perturbed the simple shear flow and led to the formation of sheath folds in the overlaying layer. This process can potentially explain how sheath folds might form in glaciotectonic sediments (e.g., Moller, 2006). In a third experiment, they tested the impact of a stiff layer that was embedded at an angle to the shear plane in the weaker matrix. The matrix again had passive marker layers for the visualization. During the deformation, the stiff layer got boudinaged, which forced the matrix to deform. At the necks, where the boudins separated, non-cylindrical folds developed in the matrix. The formation mechanisms discussed by Cobbold and Quinquis (1980) gained widespread acceptance "almost to the point where it is used unquestioningly as *the* explanation" for the formation of sheath folds (Skjernaa, 1989, p. 690).

Several authors modeled the development of sheath folds from pre-existing perturbations by means of kinematic models (Cobbold and Quinquis, 1980; Lacassin and Mattauer, 1985; Skjernaa, 1989; Mies, 1993). Such models can give information

on the amount of strain that is needed or the initial shape of the perturbation. Vollmer (1988) developed a numerical model also using a perturbation as trigger for the formation of sheath folds to explain nappe scale sheath folds.

1.3.3.2. Flow perturbation: rigid inclusion

The behavior of a rigid ellipsoidal particle in a viscous matrix is well studied (e.g., Ghosh and Sengupta, 1973; Ghosh and Ramberg, 1976; Ildefonse and Mancktelow, 1993; Arbaret et al., 2001; Dabrowski and Schmid, 2011). Marques and Cobbold (1995), Rosas et al. (2001, 2002), and Marques et al. (2008) analyzed the effect of such a rigid inclusion on the formation of sheath folds. A rigid inclusion embedded in a matrix and subjected to simple shear perturbs the laminar flow, which can lead to the formation of sheath folds (Figure 4c). In nature such inclusions can be, for example, boudins or single large mineral grains. Natural examples of sheath folds that developed around rigid inclusions were reported by Marques and Cobbold (1995), Rosas et al. (2001, 2002), and Marques et al. (2008). The same authors tested with analogue experiments the mechanisms leading to the sheath fold formation. One of the experiments conducted by Cobbold and Quinquis (1980) simulated already a similar situation. Instead of having an individual rigid inclusion, they had a sequence of boudins between which the matrix got strongly deformed and sheath folds developed. Marques and Coddold (1995), Rosas et al. (2001, 2002), and Marques et al. (2008) tested the effect of a singular rigid inclusion subjected to simple shear on the development of sheath folds. Marques and Cobbold (1995) investigated the impact of the shape of the inclusion and its position. They observed the development of sheath folds on both ends of the inclusion in the direction of the shear. The development of the folds took place in a homogeneous matrix. Rosas et al. (2001) observed that well developed sheath folds could be seen around rigid inclusions if these inclusions do not rotate in the simple shear flow. Around inclusions that rotated significantly, only minor (or no) sheath folds could be observed. Rosas et al. (2002) tested the effect of the distance between a marker layer and the inclusion on the visibility of the evolving folds. They concluded that sheath folds develop whenever the distance between the inclusion and the marker layer is less than the longer principle direction of the rigid inclusion. Marques et al. (2008) tested the impact of a viscosity ratio between the layers of the matrix. They embedded a rigid inclusion into

an actively layered matrix and sheared the experiments to a shear strain of $\gamma = 6$. They concluded that to generate a sheath fold in both the higher and lower viscosity layer, the viscosity ratio between the layers needs to be lower than 10.

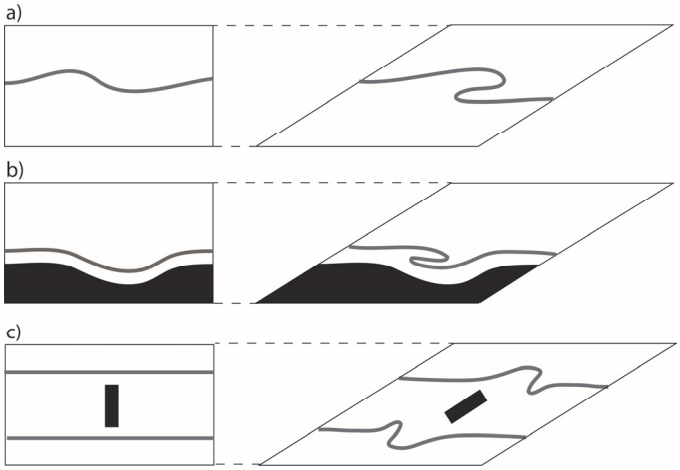

Figure 4: Schematic sketch of the different formation mechanisms of sheath folds in simple shear. a) Passive amplification of a perturbation, after Cobbold and Quinquis (1980). b) Formation of a sheath fold above a rigid and corrugated basement, after Cobbold and Quinquis (1980). c) Formation of sheath folds around a rotated rigid inclusion, after Rosas et al. (2002).

1.3.3.3. Flow perturbation: weak inclusion

Another potential formation mechanism in simple shear is the sheath fold development around weak inclusions. This idea has already been introduced for the formation of flanking structures (e.g., Grasemann et al., 2005; Exner and Dabrowski, 2010). It is suggested that a weak inclusion could act as a slip surface in simple shear, which leads to the deformation of the surrounding matrix. Exner and Dabrowski (2010) proposed that flanking structures in three-dimensions might be sheath folds. The papers included in this thesis take up this idea and show that sheath folds can indeed be formed around a weak inclusion in simple shear. This puts sheath folds in line with other structures developing through the process of slip localization on a weak inclusion where the larger scale deformation is taken up in the form of ductile folding around the slip surface such as fault-related folds (e.g., Schlische,

1995) and flanking structures (e.g., Passchier, 2001; Exner and Dabrowski, 2010; Grasemann et al., 2011).

Weak inclusions acting as slip surfaces are commonly found in nature. Weaknesses that can potentially act as slip surfaces range from cracks and veins to weak sedimentary layers and weak minerals. They are not restricted to any rock type or matrix assembly and can be found over a wide range of sizes. However, detecting a weak inclusion in the field and link it unambiguously to a sheath fold can be difficult as the inclusion might be strongly deformed and overprinted by the bulk deformation.

1.4. Application of sheath folds

Sheath folds were used to deduce kinematic and geometric information such as the strain magnitude, the bulk strain type, the shear direction, or the shear zone width. The following paragraphs deal with the individual applications of sheath folds.

1.4.1. High strain indicator

As sheath folds can often be observed in shear zones with large shear deformation they were used as a criterion for high shear strain for many years (e.g., Minnigh, 1979). This idea of sheath folds being high strain indicators is widely accepted and popular in structural geology textbooks (Kearney and Allen, 1993; Pederson and Dehler, 2005). Rosas et al. (2002) and Marques et al. (2008) have, however, shown with their analogue experiments that a strain of $\gamma \approx 5$ is sufficient to produce sheath folds. A recent study by McClelland (2011) has demonstrated that sheath folds produced by turbiditic flows can form at a shear strain of $\gamma = 1$. The essential question, which has to be answered before deciding what strain magnitude sheath folds are typical for is to determine, what *high* strain is. The opinions about what high strain is are diverse in the literature. Marques et al. (2008) state that a shear strain of $\gamma = 10$ is little when compared with high strain ductile shear zones. Mies (1993) on the other hand states that $\gamma = 10$ is a large shear strain. It seems that the measure of high strain is extremely dependent on the field the researchers work in. To say that sheath folds are high strain indicators is imprecise, as there exists no

general agreement on what high strain is. In addition, the occurrence of sheath folds cannot be linked to a specific strain value.

1.4.2. Shear sense indicators

Sheath folds are often used in the field to orient shear zones (e.g., Alsop and Carreras 2007, Kuiper et al., 2007). Fossen and Rykkelid (1990) used sheath folds not only to determine the orientation of the shear zone but also its shear sense. They observed shear-related sheath folds, which show limbs of different thicknesses. This results in a location of the center of the resulting eye-pattern in either the upper or the lower half of the structure (Figure 5). Based on their field example Fossen and Rykkelid (1990) state that by knowing the closing direction of the sheath fold cone and observing the layer thicknesses in the cross-section, the shear sense of the shear zone can be determined. For folds closing towards the observer, a thinned inverted limb (Figure 5a and d) indicates top-towards-observer sense of shear.

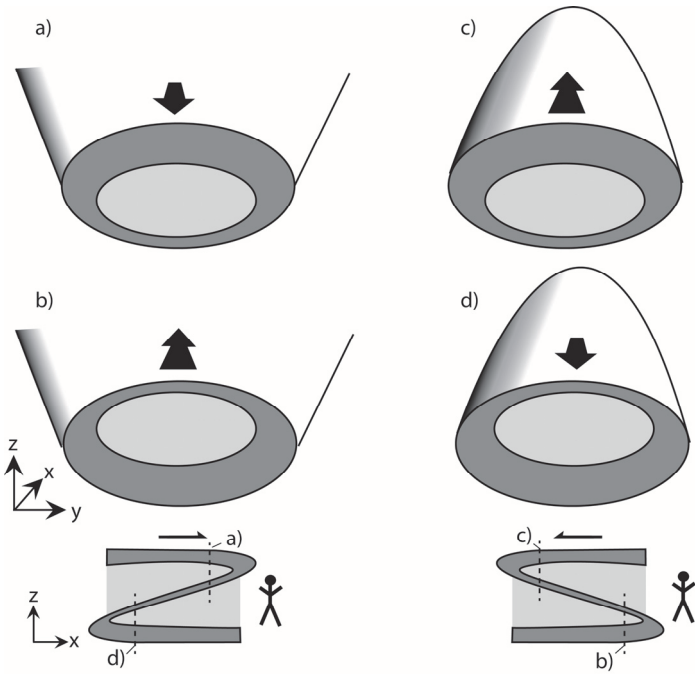

Figure 5: Sketch illustrating how the thinning/thickening of the limbs in sheath folds can give information about the shear direction after Fossen and Rykkelid (1990). a) and b) The

fold closes towards the observer. c) and d) the fold closes away from the observer. The black arrows indicate the shear direction. a) and d) show a shear direction of top towards the observer, b) and c) show a shear direction of top away from the observer.

1.4.3. Shear zone thickness indicator

When sheath folds develop in shear zones the size of the sheath fold can provide information on the minimal shear zone width (Ramsay, 1980; Lacassin and Mattauer, 1985; Skjernaa, 1989; Mies, 1993; Alsop et al., 2007). Alsop et al. (2007) stated that the maximum z-value measured in a sheath fold gives the minimum width of the shear zone. Bonamacini et al. (2011) used a large-scale sheath fold to constrain the thickness and the strain distribution within the deep crustal flow zone.

1.4.4. Bulk strain type indicator

Alsop and Holdsworth (2006) developed a classification of sheath folds based on the morphology of the eye-structure in cross-sections. Based on field observations, they linked their classification to bulk strain types. In the following paragraph, this classification and its application are introduced.

1.4.4.1. Classification

The classification by Alsop and Holdswort (2006) is based on cross-sections of sheath folds, which are perpendicular to the x-axis in the y-z plane. They approximate the closed contours or eyes with ellipses. If in such a cross-section, more than one closed contour can be seen they measure the long and the short axes of the ellipses approximating the innermost and outermost closed contour. Figure 6 shows the parameters they measured on a sheath fold cross-section. Measuring the aspect ratio of the outermost closed contour gives a value termed R_{yz}, measuring the aspect ratio of the innermost closed contour gives the value $R_{y'z'}$ (Figure 6a). Note that the interfaces and not the layers are measured, so it is possible that R_{yz} is measured on the outside of a layer and $R_{y'z'}$ on the inside of the same layer. By taking the ratio of R_{yz} and $R_{y'z'}$ a single value R' (R' = $R_{yz}/R_{y'z'}$) is defined, describing the shape of the nested closed contours. Folds showing the same aspect ratio or flatness for the outermost and innermost closed contour are called 'Analogous-eye-folds' or type A (Figure 6b). These folds have the same aspect ratio

for the inner and outermost contour ($R_{yz} = R_{y'z'}$; R' = 1). Folds that show a more rounded innermost contour and are displaying $R_{y'z'} < R_{yz}$ and R' > 1 are called 'Bull's-eye-folds' or type B. If the innermost contour is more flattened than the outermost and $R_{y'z'} > R_{yz}$ and R' < 1 the folds are called 'Cat's-eye-folds' or type C. Together with the measurements of the aspect ratios, the distance between the innermost and outermost contour along the y and z axes was measured. The ratio of this measurement (T_{yz}) gives information about the layer thickening/thinning.

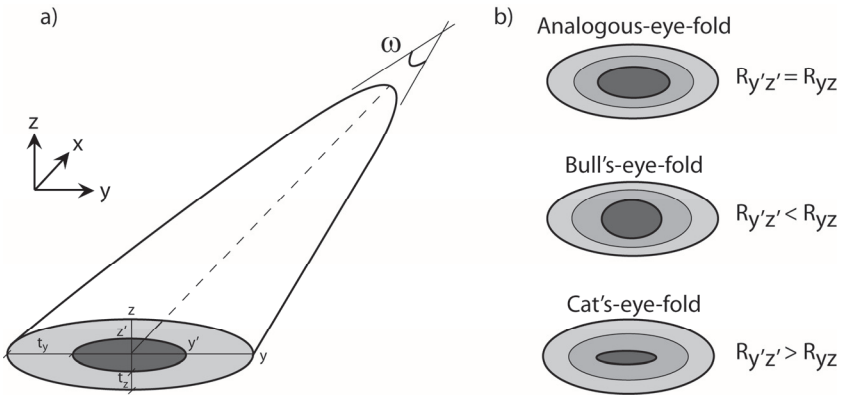

Figure 6: a) Sketch illustrating the opening angle ω and the inner and outermost closed contour used for the classification by Alsop and Holdsworth (2006). b) Classification of the eye-pattern according to Alsop and Holdsworth (2006).

1.4.4.2. Application

Using their classification of the eye-patterns described above, Alsop and Holdsworth (2006) measured R' and T_{yz} on natural sheath folds and linked the observed cross-sections to different bulk strain types. Folds generated in simple or general shear display primarily cat's-eye-structures, while folds formed in pure shear display bull's-eye-patterns. They observed that folds generated during simple shear have a mean R_{yz} value of 4.61 and a mean T_{yz} value of 3.31. Folds generated during general shear show greater thickness variations (T_{yz} = 4.35) and R_{yz} (5.76). The authors concluded that the overall variation in layer thickness and aspect ratio of the outermost closed contour increases with increasing deformation and a larger component of pure shear. R' is constant for both types of bulk strain and reflects the

original fold pattern. For folds generated in pure shear the values observed for R_{yz} as well as T_{yz} are smaller ($R_{yz} = 2.42$, $T_{yz} = 2.94$) compared to folds generated in simple or general shear.

1.4.5. Limitations of the classification and applications

The use of sheath folds as shear strain indicator is limited by two factors. As discussed in section 1.4.1 sheath folds occur over a wide range of different strains and the term 'high strain' is not clearly defined and therefore of limited use. To use sheath folds as high strain indicators might be incorrect. So far, no systematic study exists, which investigates the development of sheath folds with increasing strain.

Using the sheath folds as shear sense indicators as proposed by Fossen and Rykkelid (1990) is only possible if the sheath fold shows a layer thickening or thinning in the eye-pattern and if the closing direction of the fold is known. Until now, no studies have been carried out that investigated the thickening/thinning with respect to the shear strain, cross-section location, or formation mechanism. Their classification has not been applied to other examples.

The classification developed by Alsop and Holdswort (2006) could potentially be dependent on the observer. The outermost closed contour is a fairly clearly defined geometrical measure. The innermost closed contour, however, might be defined differently depending on the observer. No study exists that investigates the sensitivity of the classification by Alsop and Holdsworth (2006) on the location of the innermost contour. This classification is, in addition, purely empirical and has so far not been backed up by a study based on physical principles.

Using sheath folds as minimum shear zone indicators is not subject to any limitations.

1.5. Sheath fold formation around a slip surface

Section 1.3.3.3. suggests that sheath folds can form due to a weak inclusion subjected to simple shear. Section 1.4.4. lists potential problems with the existing classifications and applications of sheath folds. In this thesis, three papers are presented that investigate the formation of sheath folds around a weak inclusion and test the applicability of the existing classifications.

The following chapters will address the central questions of this thesis: Can sheath folds form around weak inclusions acting as slip surfaces? What is the impact of the slip surface orientation? What influence has the cross-section location on the structures? Can sheath folds form only in a homogeneous matrix or also in a mechanically layered one? How important is the layer thickness or the number of involved layers on the formation of the sheath folds? How much strain is required to produce sheath folds? The papers presented in this thesis address these questions with a combined analytical and experimental approach. The next section gives an overview of the used techniques, their limitations, and advantages while the subsequent sections address the questions raised above and introduces the papers in this thesis.

1.5.1. Introduction to the techniques

Both the analytical and the experimental techniques used in this thesis investigate the sheath fold formation around a weak inclusion where the deformation is simple shear. In the following two sections (1.5.1.1. and 1.5.1.2.) the used techniques are introduced. In section 1.5.1.3 the two methods are compared.

1.5.1.1. The analytical model

The analytical studies in the papers presented in chapters 2 and 4 are based on an adapted form of the external Eshelby solution, which describes the flow field around a homogeneous ellipsoidal inclusion where the elastic properties of the inclusion differ from those of the matrix (Eshelby, 1959). Exner and Dabrowski (2010) modified the original solution in such a way that it is applicable for viscous materials and a two-dimensional, inviscid inclusion. Here, one axis of the ellipsoidal inclusion tends to zero and the viscosity of the inclusion tends to zero. The slip surface is therefore a frictionless, quasi two-dimensional feature embedded in a three-dimensional homogeneous matrix block (Figure 7). The original solution was developed for an elastic medium. To modify the original solution for a viscous incompressible medium, the Poisson ratio needs to be set to ½ and the shear modulus of all the materials need to be replaced by the viscosity and the displacement has to be treated as velocity (Freeman, 1987). Into the homogeneous matrix, we place passive marker layers and apply simple shear to the model. The analytical solution is

evaluated on a cloud of points distributed in the matrix. To deform the model, the new positions of all the points are evaluated and then the points are moved accordingly. Then the shape of the inclusion is determined and the solution is re-used for the new position of the points. The inclusion keeps an elliptical shape even though it gets deformed and stretched. The model is point symmetrical with respect to the central point of the inclusion. A detailed description of the model including all the equations is presented in Exner and Dabrowski (2010).

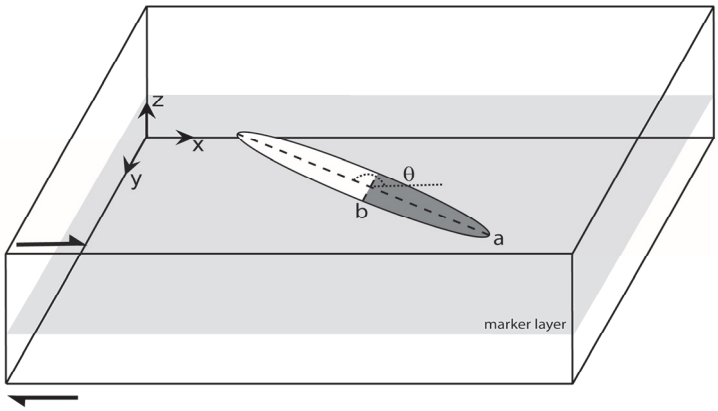

Figure 7: Model setup for the analytical model. a and b describe the main axes of the elliptical weak inclusion. θ is the angle of the initial inclusion orientation.

The model can be deformed up to an arbitrarily large simple shear strain. The deformation leads to slip on the weak inclusion and deformation of the matrix. At the tip of the inclusion, the deformation has to be taken up in the surrounding matrix, which leads to the formation of folds. To visualize the deformation the matrix contains passive marker layers. Tracing the marker layers allows studying the resulting structures in three-dimensions.

This analytical model permits for inclusion shapes that are circular or elliptical. Figure 7 shows a sketch of the initial model setup where θ represents the initial orientation angle of the inclusion and *a* and *b* are the main axes of the elliptical inclusion. The sketch shows only one marker layer but there is no limitation on the number of marker layers in the matrix. In the studies presented in this thesis, we limited the shear deformation to a shear strain of maximum $\gamma = 15$. The model is not

subject to a disrupting boundary effect. A big limitation of the model is, however, the absence of layers with different viscosities in the matrix.

1.5.1.2. The experimental model

To investigate the impact of a mechanically layered matrix, *i.e.* layers of different viscosities on the development of sheath folds, we used analogue experiments. For the experimental study, a simple shear apparatus was used, which allowed for high shear deformation. The maximum strain that could be reached with this apparatus is a simple shear strain of $\gamma = 25$. In the study presented in this thesis, we deform the experiments only to a simple shear strain of $\gamma = 6$. This strain is large enough for the formation of sheath folds, and it maximizes the volume of the experiment that is not affected by the boundaries.

The experiments are made of silicones of different viscosities, which were used as rock analogues. To produce a viscosity contrast between the silicone layers, the viscosities of the silicones were adjusted by adding iron oxide and sand (higher viscosity) or oleic acid (lower viscosity). A major challenge for the success of the experiments was the production of fine layers of silicone. A detailed account of the production process of the layering is given in chapter 3 together with the dimensional analysis of the experiments.

The weak inclusion was simulated with a cut in the silicone that was lubricated with liquid soap. We adjusted the shape of the weak inclusion to the dimensions of the experiment box. As the experiment box has a length of 40 cm, a width of 10 cm, and a height of 5 cm, we decided on an elliptical inclusion with a long axis of 4 cm and a short axis of 1.5 cm ($a/b = 2.67$). The inclusion is inserted vertically ($\theta = 90°$) into the model.

After the deformation, we cut the model into serial cross-sections perpendicular to the shear direction. Photographs of the model are taken while sections of 5 mm thickness are removed. These photographs are then used to reconstruct the shape of the sheath fold in three-dimensions. A detailed account of the experimental technique can be found in chapter 3.

Figure 8: a) Sections cut from the deformed model. The reconstruction of the models was not based on pictures of the extracted cross-sections but on pictures of the sections when they were still in the machine. b) Oleic acid and iron oxide used to change the viscosity of the silicon. c) Silicones resting to release air bubbles after the mixing with oleic acid, iron oxide, and sand. d) Double roll device used for the layer production. This rolling device is from a bakery where it was used to produce butter dough. e) Simple shear machine used for the experiments. The machine has a total length of approximately 2.5 meters.

1.5.1.3. Method comparison

The two methods used for the investigation of sheath fold formation around a weak inclusion are complementary. While the analytical model is not suited for

investigating the impact of a viscosity contrast between the layers building the matrix, the experimental model was designed to investigate this question. In comparison to the analytical model, the experimental model is subject to some but limited boundary effects such as the relatively close proximity of the walls of the experimental box and the coarse cutting spacing of the cross-sections.

To compare the two methods we performed an analytical model and an experiment with the same inclusion dimensions, inclusion orientation, number of layers scaled with the inclusion height, and total shear strain. The experiment was conducted using two differently colored silicones of equal viscosity to compare to the homogeneous analytical model. Both models were sheared to a shear strain of $\gamma = 6$. The experiment and the model show closed contours in cross-sections perpendicular to the shear direction (Figure 9). We measured the length and the dip of the deformed inclusion in both models (Figure 10). For the analytical model the evolution of the length and dip with increasing strain is shown, while for the experimental model only the final stage is displayed. The length of the crack is, in both models, normalized with the initial inclusion height. The values for the length are approximately the same in both models for the same amount of strain. The dip of the inclusion in the experiment is larger than the dip of the inclusion in the analytical model at the same final shear strain. The reason for this discrepancy might be that the confining boundary condition in the experiment prevented the inclusion from rotating to the same degree as in the analytical experiment.

Figure 9: Left side: Result from the experimental model at $\gamma = 6$, $\theta = 90°$, a/b = 2.67. Right side: corresponding analytical model.

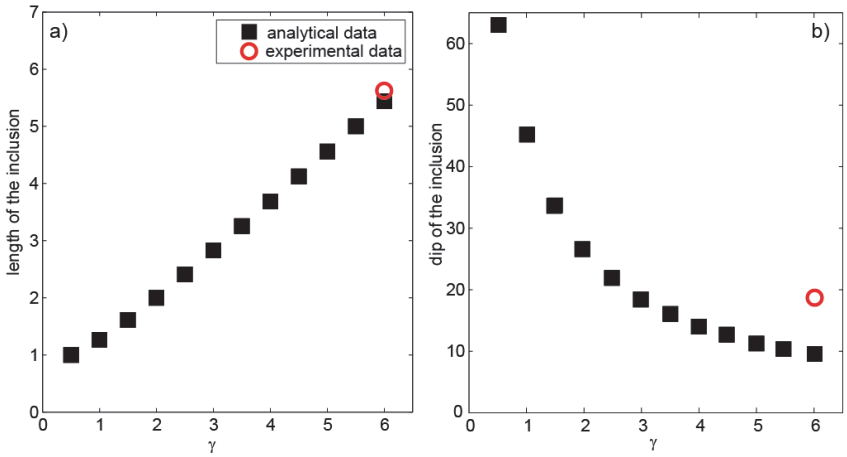

Figure 10: a) The length of the inclusion plotted against the strain for the analytical and experimental model with $\gamma = 6$, $\theta = 90°$, a/b = 2.67. b) Dip of the inclusion plotted against strain.

1.5.2. Applicability of the models to nature

Both models presented above use a linear viscous rheology to simulate the matrix and the inclusion. The flow laws in rocks are dependent on the involved mechanism, the mineral composition, and the grain size. Rocks deforming due to dislocation creep follow viscous, power flow laws (e.g., Carter, 1976). Rocks that

deform by diffusion creep show a Newtonian viscous rheology (Frost and Ashby, 1983). Using a linear viscous matrix in the models can simulate the deformation by diffusion creep. For the experiments, we used PDMS (silicone) which exhibits in its pure form (no fillers such as sand, iron oxide, or oleic acid added) a Newtonian flow behavior at strain rates commonly used in analogue laboratories (ten Grotenhuis et al., 2002). By adding fillers, the elastic component of the silicone increases. Weijermars (1986) pointed out that even though the actual deformation mechanism in the silicone differs quite strongly form the creep mechanisms in real crystalline rocks, silicone is a suitable rock analogue as the flow curve of silicone at strain rates of 10^{-3} to 10^{-1} s^{-1} is similar to the flow curves of rocks flowing at strain rates of 10^{-15} to 10^{-13} s^{-1}.

Both presented methods use a weak inclusion to perturb the simple shear flow and cause the formation of sheath folds. This inclusion behaves like a passive marker in both models. It can stretch and rotate but it cannot propagate. Natural analogues for such weak inclusions might be veins, faults, cracks, dykes, and weak sedimentary layers. While a non-propagating inclusion is suitable to simulate veins, dykes, and weak layers, it might not be obvious that it is also applicable for the simulation of faults and cracks. Means (1989) described an unfamiliar type of faults that he termed stretching faults. Such faults occur in flowing rock bodies where the wall rocks can lengthen or shorten in the slip direction. Stretching faults behave essentially passively, *i.e.* they do not propagate. Non-propagating weak inclusions have been used to describe the formation of flanking structures (Grasemann and Stuwe, 2001; Grasemann et al., 2003; Grasemann et al., 2005; Grasemann et al., 2011). Based on comparison of natural flanking structures and model results Grasemann et al. (2011) stated that the fundamental property of an inhibited fault propagation applies for the observed structures and that this is moreover a general feature of flanking structures. If we consider sheath folds to be three-dimensional flanking structures (Exner and Dabrowski, 2010) the same reasoning applies for the sheath fold formation.

Both our models deform in a monoclinic flow. Using a triclinic flow would have an impact on the resulting structures (e.g., Exner and Dabrowski, 2010; Kuiper et al., 2007). In the studies presented in this thesis we do, however, not investigate the impact of a triclinic flow.

1.6. Introduction to the papers

This thesis is a collection of papers all strongly related to each other. The individual papers are presented in chapters 2, 3, and 4. In chapter 5 some additional work is presented which does not have the format of a scientific paper. Chapter 6 contains an overall conclusion of the entire thesis and final remarks.

1.6.1. Paper I

The first paper in this thesis entitled 'Sheath fold formation around slip surfaces' (Chapter 2, published in Terra Nova) introduces the idea of sheath folds forming around slip surfaces in simple shear. Results from the three-dimensional analytical model show that the flow perturbation around a weak planar inclusion, acting as a slip surface, leads to the formation of sheath folds. In cross-sections parallel to the shear direction structures similar to flanking folds can be observed. Closed traces of marker layers are exhibited in cross-sections cut perpendicular to the shear direction in the vicinity of the slip surface tip. The impact of the location of the cross-section in x-direction on the visibility of the structures is discussed. The paper also investigates the impact of the initial orientation of the slip surface on the development of sheath folds. Three different initial orientations ($\theta = 0°$, 90°, 135°) were tested. These orientations approximate, for example, a shear plane parallel weakness, a vertical vein, or a model I fracture. We can observe for all three orientations the formation of sheath folds at the tip of the slip surface. The results from the analytical model are compared to natural sheath folds. Our model is able to reproduce the first order observations from nature such as the diversity of shapes and multiple eye-structures. In addition, we present an alternative formation mechanism for double-eye-folds.

1.6.2. Paper II

The second paper entitled 'Experimental study of sheath fold development around a weak inclusion in a mechanically layered matrix' (Chapter 3, in review in Tectonophysics) investigates the impact of a viscosity contrast between the layers building the matrix on the sheath fold development. We describe results from experiments of sheath fold formation around a weak inclusion in a matrix of silicone

layers of alternating viscosities subjected to simple shear. We investigate the impact of the viscosity ratio between the layers, which we vary from 1 to 50, and the impact of the layer thickness, which we vary from 0.5 to 6 mm. We analyze the resulting structures in cross-sections perpendicular to the shear direction. In addition to analyzing the cross-sections, we reconstruct the three-dimensional shapes of the folds. For a constant layer thickness of 1 mm, sheath folds develop for viscosity ratios up to 20. The shapes of the sheath folds, however, are dependent on the viscosity ratio. For a higher viscosity ratio, the layers are strongly deformed but no sheath fold could be determined unambiguously. The visibility of the sheath fold strongly depends on the ratio between the inclusion height and the layer thickness. Comparing the experimental sheath folds to natural examples, we can observe that our experiments capture the first order observations from nature.

1.6.3. Paper III

The third paper of this these with the title 'Analytical modeling of the morphology and internal structure of sheath folds in simple shear' (Chapter 4, prepared for Journal of Structural Geology) investigates systematically the impact of the initial slip surface configurations, such as its orientation and shape, strain, and cross-section location on the resulting folds. We employ the same analytical solution as already presented in chapter 2. We show that the aspect ratios of the closed contours are dependent on the slip surface orientation and shape, and strain. The distribution of the center of the eye-structure as a function of the cross-section location, on the other hand, is strain invariant and independent on the slip surface configurations. The center of the eye-structure is subject to change in position with respect to the outermost closed contour within one fold resulting in a large variability in layer thickness across the sheath fold length. This questions the usefulness of sheath folds as shear sense indicators. We show that the aspect ratios of the closed contours are dependent on the cross-section location. The number of sampled layers has a minimal effect on the ratio (R') of the aspect ratio of the outermost closed contour (R_{yz}) and the aspect ratio of the innermost closed contour ($R_{y'z'}$). R' is a stable measurement but it is dependent on the slip surface size and orientation. R'

values below and above 1 can be observed. Using R' measurements to deduce the bulk strain type may be erroneous.

1.6.4. Additional work

Chapter 5 is entitled 'Shear plane parallel cross-sections' and contains results from the analytical study where cross-sections parallel to the shear plane are investigated. In a short study the structures are shown resulting from cutting a sheath fold in an approximately shear plane parallel plane at different depths. Chapter 6 is entitled 'Overall conclusions' and gives an overview of the findings in this thesis and combines them to an overall conclusion.

1.7. References

Adamuszek, M., Schmid, D. W., and Dabrowski, M., 2011, Fold geometry toolbox - Automated determination of fold shape, shortening, and material properties: Journal of Structural Geology, v. 33, no. 9, p. 1406-1416.

Alsop, G. I., and Carreras, J., 2007, The structural evolution of sheath folds: A case study from Cap de Creus: Journal of Structural Geology, v. 29, no. 12, p. 1915-1930.

Alsop, G. I., and Holdsworth, R. E., 2004a, The geometry and topology of natural sheath folds: a new tool for structural analysis: Journal of Structural Geology, v. 26, no. 9, p. 1561-1589.

Alsop, G. I., and Holdsworth, R. E., 2004b, Shear zone folds: records of flow perturbation or structural inheritance?: Flow Processes in Faults and Shear Zones, v. 224, p. 177-199.

Alsop, G. I., and Holdsworth, R. E., 2006, Sheath folds as discriminators of bulk strain type: Journal of Structural Geology, v. 28, no. 9, p. 1588-1606.

Alsop, G. I., Holdsworth, R. E., and McCaffrey, K. J. W., 2007, Scale invariant sheath folds in salt, sediments and shear zones: Journal of Structural Geology, v. 29, p. 1585-1604.

Arbaret, L., Mancktelow, N. S., and Burg, J. P., 2001, Effect of shape and orientation on rigid particle rotation and matrix deformation in simple shear flow: Journal of Structural Geology, v. 23, no. 1, p. 113-125.

Balk, R., 1953, Salt structure of Jefferson Island salt dome, Iberia and Vermillion parishes, Louisiana: Aapg Bulletin-American Association of Petroleum Geologists, v. 37, no. 11, p. 2455-2474.

Berlenbach, J. W., and Roering, C., 1992, Sheath-fold-like structures in pseudotachelytes: Journal of Structural Geology, v. 14, no. 7, p. 847-856.

Biot, M. A., 1957, Folding instability of a layered viscoelastic medium under compression: Proceedings of the Royal Society of London Series a-Mathematical and Physical Sciences, v. 242, no. 1231, p. 444-454.

Biot, M. A., 1961, Theory of folding of stratified viscoelastic media and its implications in tectonics and orogenesis: Geological Society of America Bulletin, v. 72, no. 11, p. 1595-1620.

Biot, M. A., Ode, H., and Roever, W. L., 1961, Experimental verification of the theory of folding of stratified viscoelastic media: Geological Society of America Bulletin, v. 72, no. 11, p. 1621-&.

Bonamici, C. E., Tikoff, B., and Goodwin, L. B., 2011, Anatomy of a 10 km scale sheath fold, Mount Hay ridge, Arunta Region, central Australia: The structural record of deep crustal flow: Tectonics, v. 30.

Branney, M. J., Barry, T. L., and Godchaux, M., 2004, Sheathfolds in rheomorphic ignimbrites: Bulletin of Volcanology, v. 66, no. 6, p. 485-491.

Carey, S. W., 1962, Folding: J. Alberta Soc. Petrol. Geol., v. 10, p. 95-144.

Carosi, R., and Oggiano, G., 2002, Transpressional deformation in northwestern Sardinia (Italy): insights on the tectonic evolution of the Variscan Belt: Comptes Rendus Geoscience, v. 334, no. 4, p. 287-294.

Carreras, J., Druguet, E., and Griera, A., 2005, Shear zone-related folds: Journal of Structural Geology, v. 27, no. 7, p. 1229-1251.

Carreras, J., Estrada, A., and White, S., 1977, Effects of folding on c-axis fabrics of a quertz mylonite: Tectonophysics, v. 39, no. 1-3, p. 3-24.
Carter, N. L., 1976, Steady-state flow of rocks: Reviews of Geophysics, v. 14, no. 3, p. 301-360.
Chapple, W. M., 1968, A mathematical theory of finite-amplitude rock-folding: Geological Society of America Bulletin, v. 79, no. 1, p. 47-&.
Cobbold, P. R., and Quinquis, H., 1980, Development of sheath folds in shear regimes: Journal of Structural Geology, v. 2, no. 1-2, p. 119-126.
Crispini, L., and Capponi, G., 1997, Quartz fabric and strain partitioning in sheath folds: an example from the Voltri group (western Alps, Italy): Journal of Structural Geology, v. 19, no. 9, p. 1149-1157.
Dabrowski, M., and Schmid, D. W., 2011, A rigid circular inclusion in an anisotropic host subject to simple shear: Journal of Structural Geology, v. 33, no. 7, p. 1169-1177.
Davis, G. H., and Reynolds, S. J., 1984, Structural Geology of Rocks and Regions, John Wiley & Sons, Inc.
de Beaumont, E., 1852, Notice sur le systeme des montagnes.
de Saussure, H. B., 1796, Voyages dans les Alpes.
Dieterich, J., 1969, Origin of cleavage in folded rocks: American Journal of Science, v. 267, no. 2.
Dixon, J. M., and Summers, J. M., 1985, Recent developments in centrifuge modeling of the tectonic processes- Equiplent, model construction techniques and rheology of model meterials: Journal of Structural Geology, v. 7, no. 1, p. 83-102.
Eshelby, J. D., 1959, The elastic field outside an ellipsoidal inclusion: Proceedings of the Royal Society of London Series a-Mathematical and Physical Sciences, v. 252, no. 1271, p. 561-569.
Exner, U., and Dabrowski, M., 2010, Monoclinic and triclinic 3D flanking structures around elliptical cracks: Journal of Structural Geology, v. 32, no. 12, p. 2009-2021.
Ez, V., 2000, When shearing is a cause of folding: Earth-Science Reviews, v. 51, no. 1-4, p. 155-172.
Fletcher, R. C., 1991, Three-dimensional folding of an embedded viscous layer in pure shear: Jpurnal of Structural Geology, v. 13, no. 1, p. 87-96.
Fletcher, R. C., 1974, Wavelenth selection in folding of a single layer with power-law rheology: American Journal of Science, v. 274, no. 9, p. 1029-1043.
Fletcher, R. C., 1977, Folding of a single viscous layer - Exact inifintesimal amplitude solution: Tectonophysics, v. 39, no. 4, p. 593-606.
Fossen, H., 2010, Structural Geology, Cambridge, UK, Cambridge, University Press.
Fossen, H., and Rykkelid, E., 1990, Shear zone structures in the Oygarden area, west Norway: Tectonophysics, v. 174, no. 3-4, p. 385-397.
Freeman, B., 1987, The behavior of deformable ellipsoidal particles in 3-dimensional slow flows - Implications for geological strain analysis: Tectonophysics, v. 132, no. 4, p. 297-309.
Frehner, M., and Schmalholz, S. M., 2006, Numerical simulations of parasitic folding in multilayers: Journal of Structural Geology, v. 28, no. 9, p. 1647-1657.

Frost, H. J., and Ashby, M. F., 1983, Deformation-Mechanism Maps: the Plasticity and Creep of Metals and Ceramics, Oxford, Pergamon.

George, A. D., 1990, Deformation processes in an accretionary prism- A study from the Torlesse Terrane of New-Zealand: Journal of Structural Geology, v. 12, no. 5-6, p. 747-759.

Ghosh, S. K., Hazra, S., and Sengupta, S., 1999, Planar, non-planar and refolded sheath folds in the Phulad Shear Zone, Rajasthan, India: Journal of Structural Geology, v. 21, no. 12, p. 1715-1729.

Ghosh, S. K., and Ramberg, H., 1968, Buckling experiments on intersecting fold patterns: Tectonophysics, v. 5, no. 2, p. 89-&.

Ghosh, S. K., and Ramberg, H., 1976, Reorientation of inclusions by combination of pure shear and simple shear: Tectonophysics, v. 34, no. 1-2, p. 1-70.

Ghosh, S. K., and Sengupta, S., 1973, Compression and simple shear of test models with rigid and deformable inclusions: Tectonophysics, v. 17, no. 1-2, p. 133-175.

Ghosh, S. K., and Sengupta, S., 1984, Successive development of plane noncylindrical folds in progressive deformation: Journal of Structural Geology, v. 6, no. 6, p. 703-709.

Goscombe, B., 1991, Intense noncoaxial shear and the development of mega-scale sheath folds in the Arunta block, Central Australia: Journal of Structural Geology, v. 13, no. 3, p. 299-318.

Grasemann, B., Exner, U., and Tschegg, C., 2011, Displacement-length scaling of brittle faults in ductile shear: Journal of Structural Geology, v. 33, no. 11, p. 1650-1661.

Grasemann, B., Martel, S., and Passchier, C., 2005, Reverse and normal drag along a fault: Journal of Structural Geology, v. 27, no. 6, p. 999-1010.

Grasemann, B., and Stuwe, K., 2001, The development of flanking folds during simple shear and their use as kinematic indicators: Journal of Structural Geology, v. 23, no. 4, p. 715-724.

Grasemann, B., Stuwe, K., and Vannay, J. C., 2003, Sense and non-sense of shear in flanking structures: Journal of Structural Geology, v. 25, no. 1, p. 19-34.

Grasemann, B., Wiesmayr, G., Draganits, E., and Fusseis, F., 2004, Classification of refold structures: Journal of Geology, v. 112, no. 1, p. 119-125.

Hall, J., 1815, On the vertical position and convolutions of certain strata and their relation with granite: Transactions Royal Society Edinburgh, no. 7, p. 79-108.

Hall, J., 1843, Geology of New York, Part IV, Encyclopaedis Britannica.

Hansen, E., 1971, Strain facies, Springer-Verlag.

Harding, T. P., 1973, Newport-Inglewood Trend, California - Example of wrenching style of deformation: American Association of Petroleum Geologists Bulletin, v. 57, no. 1, p. 97-116.

Harms, T. A., Burger, H. R., Blednick, D. G., Cooper, J. M., King, J. T., Owen, D. R., Lowell, J., Sincock, M. J., Kranenburg, S. R., Pufall, A., and Picornell, C. M., 2004, Character and origin of Precambrian fabrics and structures in the Tobacco Root Mountains, Montana: Geological Society of America Special Papers, v. 377, p. 203-226.

Henderson, J. R., 1981, Structural-analysis of sheath folds with horizontal x-axis, northeast Canada: Journal of Structural Geology, v. 3, no. 3, p. 203-210.

Hibbard, J., and Karig, D. E., 1987, Sheath-like folds and progressive fold deformation in tertiary sedimentary-rocks of the Shimanto accretionary complex, Japan: Journal of Structural Geology, v. 9, no. 7, p. 845-857.

Holdsworth, R. E., and Roberts, A. M., 1984, Early curvilinear fold structures and strain in the moine of the Glen Garry Region, Inverness-Shire: Journal of the Geological Society, v. 141, no. MAR, p. 327-338.

Hudleston, P. J., and Treagus, S. H., 2010, Information from folds: A review: Journal of Structural Geology, v. 32, no. 12, p. 2042-2071.

Hutton, J., 1788, Theory of the earth; or an investigation of the laws observable in the composition, dissolution, and restoration of lan upon the globe: Transactions of the Royal Society of Edinburgh, v. I, no. II, p. 209-304.

Ildefonse, B., and Mancktelow, N. S., 1993, Deformation around rigid particles - the influence of slip at the particle matrix onterface: Tectonophysics, v. 221, no. 3-4, p. 345-359.

Jiang, D. Z., and Williams, P. F., 1999, When do dragfolds not develop into sheath folds in shear zones?: Journal of Structural Geology, v. 21, no. 6, p. 577-583.

Kearney, P., and Allen, P. A., 1993, The encyclopedia of the solid earth sciences, Oxford, Blackwell Science Ltd.

Kluiving, S. J., Rappol, M., and Vanderwateren, D., 1991, Till stratigraphy and ice movements in eastrenOverijssel, The Netherlands: Boreas, v. 20, no. 3, p. 193-205.

Kuiper, Y. D., Jiang, D. Z., and Lin, S. F., 2007, Relationship between non-cylindrical fold geometry and the shear direction in monoclinic and triclinic shear zones: Journal of Structural Geology, v. 29, no. 6, p. 1022-1033.

Kupfer, D. H., 1976, Shear zones inside Gulf coast salt stocks help to delineate spines of movement: Aapg Bulletin-American Association of Petroleum Geologists, v. 60, no. 9, p. 1434-1447.

Lacassin, R., and Mattauer, M., 1985, Kilometer-scale sheath fold at Mattmark and implications for transport direction in the Alps: Nature, v. 315, no. 6022, p. 739-742.

Mandal, N., Mitra, A. K., Sarkar, S., and Chakraborty, C., 2009, Numerical estimation of the initial hinge-line irregularity required for the development of sheath folds: A pure shear model: Journal of Structural Geology, v. 31, no. 10, p. 1161-1173.

Marques, F. G., and Cobbold, P. R., 1995, Development of highly noncylindrical folds around rigid ellipsoidal inclusions in bulk simple shear regimes - Natural examples and experimental modeling: Journal of Structural Geology, v. 17, no. 4, p. 589-&.

Marques, F. O., Guerreiro, S. M., and Fernandes, A. R., 2008, Sheath fold development with viscosity contrast: Analogue experiments in bulk simple shear: Journal of Structural Geology, v. 30, no. 11, p. 1348-1353.

McClelland, H. L. O., Woodcock, N. H., and Gladstone, C., 2011, Eye and sheath folds in turbidite convolute lamination: Aberystwyth Grits Group, Wales: Journal of Structural Geology, v. 33, no. 7, p. 1140-1147.

Means, W. D., 1976, Stress and strain Basic concepts of continuum mechanics for geologists, New York Heidelberg Berlin, Springer-Verlag.

Means, W. D., 1989, Stretching faults: Geology, v. 17, no. 10, p. 893-896.

Mies, J. W., 1993, Structural-analysis of sheath folds in the Sylacauga-Marble-Group, Talladega Salte Belt, southern Appalachians: Journal of Structural Geology, v. 15, no. 8, p. 983-993.
Minnigh, L. D., 1979, Structural-analysis of sheath-fold in meta-chert from the Western Italian Alps: Journal of Structural Geology, v. 1, no. 4, p. 275-282.
Moller, P., 2006, Rogen moraine: an example of glacial reshaping of pre-existing landforms: Quaternary Science Reviews, v. 25, no. 3-4, p. 362-389.
Morales, L. F. G., Casey, M., Lloyd, G. E., and Williams, D. M., 2011, Kinematic and temporal relationships between parallel fold hinge lines and stretching lineations: A microstructural and crystallographic preferred orientation approach: Tectonophysics, v. 503, no. 3-4, p. 207-221.
Nicholson, R., 1963, Eyed folds and interfenence patterns in the Sokumfjell marble group, northern Norway: Geol. Mag., v. 100, p. 59-70.
Nicolas, A., and Boudier, F., 1975, Kinematic interpretation of folds in alpine-type peridotites: Tectonophysics, v. 25, no. 3-4, p. 233-260.
Parrish, D. K., 1973, Non-linear finite-element fold model: American Journal of Science, v. 273, no. 4, p. 318-334.
Passchier, C. W., 2001, Flanking structures: Journal of Structural Geology, v. 23, no. 6-7, p. 951-962.
Pederson, J. L., and Dehler, C. M., 2005, Interior Western United States, Boulder, Colorado, USA, Geological Society of America.
Philippon, M., Brun, J. P., and Gueydan, F., 2009, Kinematic records of subduction and exhumation in the Ile de Groix blueschists (Hercynian belt; Western France): Journal of Structural Geology, v. 31, no. 11, p. 1308-1321.
Quinquis, H., Audren, C., Brun, J. P., and Cobbold, P. R., 1978, Intense progressive shear in Lie de Groix bluschists and compatibility with subduction or obduction: Nature, v. 273, no. 5657, p. 43-45.
Quirke, T. T., and Lacy, W. C., 1941, Deep-zone dome and basin structures: Journal of Geology, v. 49, no. 6, p. 589-609.
Ramberg, H., 1963, Fluid dynamics of viscous buckling applicable to folding of layered rocks: Bulletin of the Americal Association of Petroleum Geologists, v. 47, p. 484-505.
Ramsay, J. G., 1958, Superimposed folding at Loch Monar, Inverness-shire and Ross-shire: Q. Jl geol. Soc. Lond., v. 113, p. 270-307.
Ramsay, J. G., 1967, Folding and fracturing of rocks, London, Imperial College of Scienece and Technilogy.
Ramsay, J. G., 1980, Shear zone geometry - A review: Journal of Structural Geology, v. 2, no. 1-2, p. 83-99.
Ramsay, J. G., and Huber, M. J., 1987, The techniques of modern structural geology. Volume 2: Folds and fractures, Academic Press, London.
Ranalli, G., 1995, Rheology of the Earth, London, Chapman & Hall, Second ed.
Rosas, F., Marques, F. G., Coelho, S., and Fonseca, P., 2001, Sheath fold development in bulk simple shear: Analogue modeling of natural examples from the Southern Iberian Variscan fold belt: In: Koyi, H. A., Mancktelow N. (Eds.), Tectonic Modeling: A Volume in Honor of Hans Ramberg. Geological Society of America Memoir, v. 139, p. 103-115.

Rosas, F., Marques, F. O., Luz, A., and Coelho, S., 2002, Sheath folds formed by drag induced by rotation of rigid inclusions in viscous simple shear flow: nature and experiment: Journal of Structural Geology, v. 24, no. 1, p. 45-55.
Scheuchzer, J., 1718, Helvetiae stoicheiographia, Zurich.
Schlische, R. W., 1995, Geometry and origin of fault-related folds in extensional settings: Aapg Bulletin-American Association of Petroleum Geologists, v. 79, no. 11, p. 1661-1678.
Schmid, D. W., Dabrowski, M., and Krotkiewski, M., 2008, Evolution of large amplitude 3D fold patterns: A FEM study: Physics of the Earth and Planetary Interiors, v. 171, no. 1-4, p. 400-408.
Searle, M. P., and Alsop, G. I., 2007, Eye-to-eye with a mega-sheath fold: A case study from Wadi Mayh, northern Oman Mountains: Geology, v. 35, no. 11, p. 1043-1046.
Skjernaa, L., 1989, Tubular folds and sheath folds - Definitions and conceptual models for their development, with examples from the Grapesvare Area, Northern Sweden: Journal of Structural Geology, v. 11, no. 6, p. 689-703.
Smith, R. B., 1977, Formation of folds, boudinage, and mullions in non-newtonian materials: Geological Society of America Bulletin, v. 88, no. 2, p. 312-320.
Smith, R. B., 1979, Folding in a strongly non-newtonian layer: American Journal of Science, v. 279, no. 3, p. 272-287.
Srivastava, D. C., 2011, Geometrical similarity in successively developed folds and sheath folds in the basement rocks of the northwestern Indian Shield: Geological Magazine, v. 148, no. 1, p. 171-182.
Stauffer, M. R., and Lewry, J. F., 1993, Regional setting and kinematic features of the needle falls shear zone, Trans-Hudson Orogen: Canadian Journal of Earth Sciences, v. 30, no. 7, p. 1338-1354.
Steno, N., 1669, De solido intra solidum naturaliter contento dissertationis prodromus.
Talbot, C. J., and Jackson, M. P. A., 1987, Internal kinematics of slat diapirs: Aapg Bulletin-American Association of Petroleum Geologists, v. 71, no. 9, p. 1068-1093.
ten Grotenhuis, S. M., Piazolo, S., Pakula, T., Passchier, C. W., and Bons, P. D., 2002, Are polymers suitable rock analogs?: Tectonophysics, v. 350, p. 35-47.
Thomas, G. S. P., and Summers, A. J., 1984, Glacio-dynamic structures from the Blackwater formation, Co Wexfors, Ireland: Boreas, v. 13, no. 1, p. 5-12.
Twiss, R. J., and Moores, E. M., 2007, Structural Geology, New York, W. H. Freeman and Company.
Van der Pluijm, B., and Marshak, S., 2004, Earth structure, New York, Norton and Company, Inc.
Vollmer, F. W., 1988, A computer-model of sheath-nappes formed during crustal shear in the Western Gneiss Region, central norwegian Caledonides: Journal of Structural Geology, v. 10, no. 7, p. 735-743.
Wegener, A., 1929, Die Entstehung der Kontinente und Ozeane, Braunschweig.
Weijermars, R., 1986, Flow behaviour and physical chemistry of bouncing putties and related polymers in view of tectonic laboratory applications: Tectonophysics, v. 124, p. 325-358.
Willis, B., 1894, The mechanics of Appalachian structure.

3. Experimental study of sheath fold development around a weak inclusion in a mechanically layered matrix

3.1. Abstract

Sheath folds are highly non-cylindrical structures. They are common in shear zones. In cross-sections perpendicular to the shear direction, folded layers appear as closed contours ("eye-structures"). The mechanisms of development of sheath folds are a subject of debate. Here we describe experiments on sheath fold formation around a weak inclusion in a matrix consisting of silicone layers of alternating viscosity. The main experimental variables were the viscosity ratio (from 1 to 50) and the thickness of the layers (from 0.5 to 6 mm). We deformed the models in a simple shear apparatus to a shear strain of $\gamma = 6$. We cut serial cross-sections, perpendicular to the shear direction, and reconstructed the folds in 3D. All experiments with a weak inclusion resulted in strong deformation of the layers. For an initial layer thickness of 1 mm, sheath folds formed, no matter what was the viscosity ratio. However, for larger viscosity ratios, the sheath folds formed at larger angles with respect to the shearing plane, were less elongate, and had wider opening angles. In general, the visibility of a sheath fold strongly depended on the aspect ratio between the inclusion height and the layer thickness: we observed sheath folds for a ratio larger than 7.5. The experiments reproduced the first-order features of natural

Jacqueline E. Reber[1], Olivier Galland[1], Peter R. Cobbold[2], Christian Le Carlier de Veslud[2]

[1]Physics of Geological Processes, University of Oslo, Norway

[2]Geosciences (UMR6118), CNRS et Université de Rennes 1, France

Accepted in Tectonophysics, revisions not included

sheath folds. In the experiments, sheath folds readily nucleated around weak inclusions, therefore we expect this to be a common process in nature.

3.2. Introduction

Sheath folds are quasi-conical structures with rounded apices (Figure 1a) (Hansen, 1971; Quinquis et al., 1978; Ramsay, 1980; Skjernaa, 1989). Ramsay and Huber (1987) defined sheath folds as having an opening angle of < 90° (Figure 2). Sheath folds are three-dimensional structures and some examples crop out fully as such (Quinquis et al., 1978). In general, however, sheath folds are more readily visible on cross-sections perpendicular to the shear direction (e.g., Alsop and Holdsworth, 2006), where the layers show closed contours (Figure 1b). Although these structures are now called sheath folds, earlier terms were ‘domes and basins’ (Quirke and Lacy, 1941), ‘closed folds’ (Balk, 1953) or ‘eyed folds’ (Nicholson, 1963). Sheath folds occur in many rock types, such as metamorphic rocks (e.g., Carreras et al., 1977; Quinquis et al., 1978; Philippon et al., 2009), soft sediment (e.g., George, 1990; McClelland et al., 2011), or ignimbrite (Branney et al., 2004). In length they may be from less than one millimeter (Berlenbach and Roering, 1992) to more than one kilometer (Lacassin and Mattauer, 1985). Alsop et al. (2007) demonstrated that sheath folds are to a significant degree scale-invariant. Carreras et al. (1977) and subsequent workers (e.g., Quinquis et al., 1978; Alsop and Holdsworth, 2006; Fossen and Rykkelid, 1990; Minnigh, 1979) associated sheath folds with shear zones and used their shapes to infer strain magnitude (e.g. Alsop and Holdsworth, 2004), shear sense (Fossen and Rykkelid, 1990) or bulk strain type (Alsop and Holdsworth, 2006).

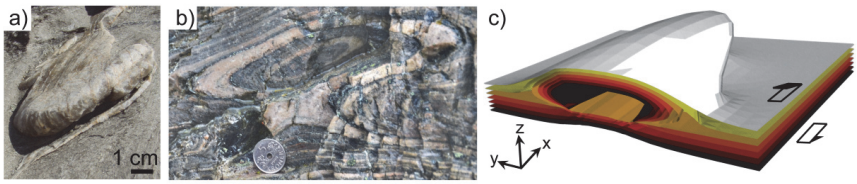

Figure 1: a) Photograph of quartz layer, cropping out as sheath fold, Cap de Creus, Spain. b) Photograph of sheath fold as eye-structure in quartzite layers on cross-section perpendicular

to shear direction, Oppdal, Norway. c) Three-dimensional diagram of sheath fold according to analytical model of Reber et al. (2012). Arrows indicate the shear direction.

A simple approach to studying sheath folds is through detailed description and classification of their shapes (e.g., Skjernaa, 1989; Alsop and Holdsworth, 2006). Such an approach, however, provides few insights into the kinematics and mechanics of their development. Simple theories of buckling (e.g., Biot, 1957) are two-dimensional and predict cylindrical folds, so that they are not applicable to sheath folds. Several studies have suggested that sheath folds arise during a flow perturbation in simple shear. Such a perturbation may be due to (1) a local undulation in otherwise planar and passive layering (Cobbold and Quinquis, 1980), (2) a rigid inclusion, such as a boudin (Marques and Cobbold, 1995; Marques et al., 2008; Rosas et al., 2002), or (3) a weak inclusion, such as a crack or vein (Exner and Dabrowski, 2010; Reber et al., 2012). The bulk deformation may also involve components of constriction or flattening (Ez, 2000; Mandal et al., 2009). In nature, however, the causes of sheath fold development may not be discernible, as the bulk deformation may have overprinted the initial perturbation, or the resulting sheath fold and the triggering objects may have separated during deformation.

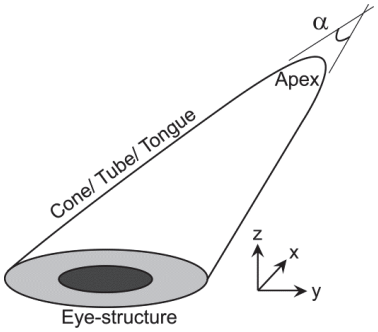

Figure 2: Sketch of a sheath fold (α denotes the opening angle of cone).

Early studies of the mechanics of sheath folds were mainly experimental, but some recent ones have been numerical (Mandal et al., 2009) or analytical (Reber et al., 2012). Most former studies assumed a homogeneous matrix for the development of sheath folds. In nature, however, many sheath folds in rocks involve layers of

contrasting viscosities (e.g., Alsop and Holdsworth, 2006; Morales et al., 2011). Marques et al. (2008) tested the effect of a mechanically layered matrix on sheath fold development around a rigid inclusion. They concluded that sheath folds do not develop when the viscosity ratio between the layers is larger than 10. However, in their experiments the ratio between the inclusion size and the layer thickness was constant, whereas Dabrowski and Schmid (2011) argued that this parameter controls the visibility of the evolving structures.

In this paper, we present an experimental study of sheath fold development in a mechanically layered matrix of silicone around a weak inclusion. Our experimental setup consisted of a simple shear apparatus. In a systematic manner, we tested the effects of (1) the viscosity ratio between the layers, and (2) the aspect ratio between the size of the inclusion and the layer thickness.

3.2.1. Experimental procedure

Typically, the preparation and running of each experiment required 3 to 4 days.

3.2.1.1. Model material

To build the matrix we used polydimethyl-siloxane (PDMS-DC SGM36, Dow Corning, Great Britain, further referred to as silicone), which is a suitable model material for the strain rates such as those in our experiments (ten Grotenhuis et al., 2002; Weijermars, 1986).

For the pure silicone, we measured a viscosity of 3.5×10^4 Pa s at 21°C. To test the effect of mechanical layering on the development of sheath folds, we needed silicones of different viscosities. To increase the viscosity, we mixed the pure silicone with inert fillers, such as fine-grained sand or iron-oxide (Weijermars, 1986) thus obtaining a maximal viscosity of 5.3×10^5 Pa s. Conversely, to decrease the viscosity we mixed the pure silicone with oleic acid (Weijermars, 1986), so obtaining a minimal viscosity of 7.2×10^3 Pa s. Thus, this procedure allowed us to produce a viscosity ratio up to 50. For details on the viscosity measurements see Appendix A.

To simulate the weak inclusion, we used a liquid soap (Arma®, Marseille). We measured the viscosity of the soap, using the same rotary viscometer as

described by Galland et al. (2006) for low viscosity fluids, and obtained a value of approximately 1 Pa s at room temperature.

3.2.1.2. Apparatus

We conducted the experiments in the simple shear machine used by Cobbold and Quinquis (1980) (Figure 3a). The model lies in an experimental chamber, 40 cm long, 10 cm wide, and 5 cm high (Figure 3b). The top and bottom plates of the machine move at the same speed, but in opposite directions. The end walls, initially perpendicular to the shear direction (y-z plane) consist of stacks of sliding plates (Figure 3b). These distribute the shear strain evenly across the thickness of the model. Finally, the vertical boundaries, parallel to the shear direction and perpendicular to the shearing planes, are stationary. To reduce the friction on these boundaries, we lubricated them with liquid soap. In a homogeneous model, such boundary conditions should result in a nearly uniform strain. For all the experiments, we applied a constant strain rate of 3.5×10^{-4} s^{-1} and deformed the models up to a shear strain of $\gamma = 6$.

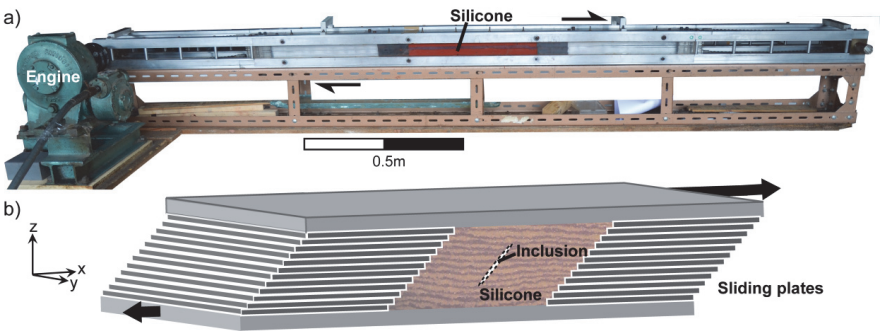

Figure 3: a) Photograph of simple shear apparatus. Lateral walls are stationary and transparent. Stack of sliding plates provides confinement at ends of model. Engine applies constant velocity via confining plates at top and bottom. b) Diagram of experimental chamber (40 cm x 10 cm x 5 cm). Model consists of layers of silicone. In centre of model is weak inclusion of liquid soap. Model deforms to shear strain of $\gamma = 6$.

3.2.1.3. Construction of models

We made the models out of fine layers of silicone, of alternating viscosities (Figure 3b). We aimed to test the effect of the layer thickness, and especially to produce very thin layers. To do so, we adopted the following technique of Dixon and Summers (1985).

(1) We individually prepared 8 mm-thick plates of two silicones using a double-roller device commonly used in bakeries. To prevent the silicone from sticking to the rollers and the underlying surface, we sprayed a very thin film of water on a thin plastic sheet, before placing the layer of silicone. We also wetted the upper surface of the silicone to prevent it from sticking to the upper roller. (2) When the required thickness was reached, we dried the silicone plates and stacked them. The two silicone surfaces adhered as soon as they were in contact so that slip between the silicone layers became impossible. (3) The two-layer stack was then rolled to a final thickness of 8 mm, whereupon each layer acquired a uniform thickness of 4 mm. (4) We then cut the two-layer stack into two pieces of equal sizes, and placed them on top of each other. (5) The stack was rolled once more to a total thickness of 8 mm. It contained now 4 layers of 2 mm thickness. (6) We repeated this procedure until we reached the desired layer thickness. The preparation of the thin silicone layers is essentially the same as the preparation of butter dough.

Using this procedure, Dixon and Summers (1985) claimed that they could attain a layer thickness of 20 μm. The finest layering that we achieved was 0.5 mm. We could not produce thinner layers, as the sand grains (Ø25 μm) used as inert fillers interfered with the thin layers.

The viscosity ratio had a negligible effect on the preparation procedure described above. We assume that if the rolling is faster than the relaxation time of the individual silicones, they thin equally. During the experiments, the applied strain rates were much lower, and the silicones of different viscosities behaved differently. This technique, however, reached its limits when the viscosity ratio between the silicones was 50 or higher. In this case, the layer did not thin equally anymore.

Using the above technique, we prepared six silicone multilayers (each of 8 mm total thickness), and cut them to the length and width of the experimental chamber. We placed all but one multilayer in the experimental chamber. Then, we

introduced a weak inclusion, in the following way. (1) We poured liquid soap into an elliptical mould, 4 cm long, 1.5 cm high (the inclusion height, *a*) and 1 mm thick. (2) We froze the mould. (3) We made a vertical cut with a knife in the middle of the model. (4) We extracted the soap tablet from the mould and inserted it into the cut. (5) Before the soap melted, we placed the last silicone multilayer on top, so that it sealed in the soap. In this way, the inclusion became an almost planar feature, which later acted as a slip surface during deformation of the model.

3.2.1.4. Observation of the deformed model

After each experiment, we placed the model in a deep-freezer for 24 hours. This made subsequent cutting easier, because the viscosity of the silicone had increased by several orders of magnitude.

We cut the model into serial cross-sections perpendicular to the shear direction at regular intervals of 5 mm and then photographed them. The cutting process led to some unwanted deformation in the model (Figure 4a). So as to analyze the structures meaningfully, we first restored the slices to their original configurations. For this purpose, we designed an automatic restoration procedure using the Matlab function *interp1*. The restoration algorithm takes every column of pixels in the photograph and stretches it to its original height, (5 cm), so that the upper surface of the model becomes once again horizontal (Figure 4 c). Finally, we considered only those areas that were free of shadows (Figure 4c, dashed box).

	Definition of parameters	Dimensions
a	Inclusion height	m
b	Layer thickness	m
d	Sheath fold depth	m
h	Sheath fold height	m
w	Sheath fold width	m
α	Opening angle	degrees
γ	Strain	
$\dot{\varepsilon}$	Strain rate	s^{-1}
η_1	Viscosity weak silicone	Pa s
η_2	Viscosity strong silicone	Pa s
η_c	Viscosity crack	Pa s
σ	Stress	Pa

Table 1: Symbols and units of the parameters in this paper.

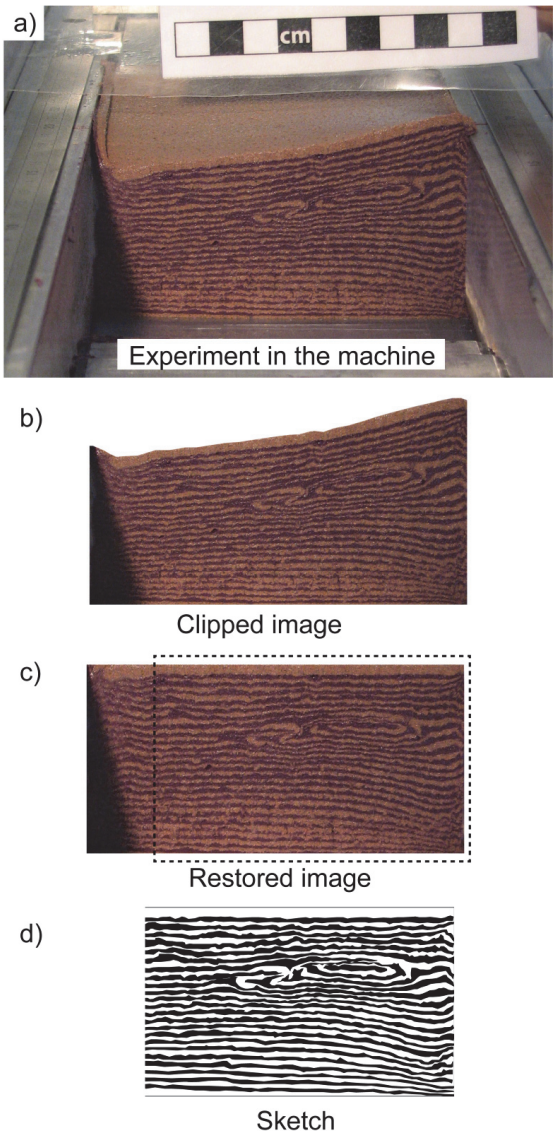

Figure 4: a) Oblique photograph of experiment V4 (viscosity ratio = 20, layer thickness = 1 mm) after sectioning. Upper confining plate has been removed. b) Clipped photograph. View is parallel to shear direction and perpendicular to section c) Same clipped image after restoration to original shape using Matlab script. Dashed box indicates area of analysis of folds. d) Sketch of restored section.

3.2.1.5. Dimensional analysis

The principle of any scaling procedure is to identify dimensionless numbers that describe the properties, kinematics and kinetics of the modeled processes (Barenblatt, 2003). These ratios can be defined in both the model and its natural prototype on the basis of the governing parameters of the processes. For our experiments, geometric input parameters were the inclusion height (*a*) and the layer thickness (*b*) (Tab. 1). In each experiment, we used two silicones of different viscosities η_1 (weak) and η_2 (strong); η_c denotes the viscosity of the liquid soap of the inclusion, γ and $\dot{\varepsilon}$ denote the applied strain and strain rate, respectively, while σ (Pa) denotes the stress.

Thus there were 8 variable parameters, and 3 of them had independent dimensions. According to the Buckingham-Π theorem (Barenblatt, 2003), five dimensionless numbers are necessary.

A first obvious parameter is strain, which is dimensionless:

$$\Pi_1 = \gamma . \tag{1}$$

Previous work has shown that sheath folds can develop at a shear strain of $\gamma \approx 1$ (McClelland et al., 2011). We therefore expect $\gamma = 6$ to be sufficient to produce sheath folds. As we keep Π_1 constant, we will not investigate its effect any further.

A second dimensionless parameter is the geometric ratio between the inclusion height *a* and the layer thickness *b*:

$$\Pi_2 = \frac{a}{b} . \tag{2}$$

In our experiments, the inclusion height (*a*) was constant (15 mm) and the layer thickness (*b*) was in the range of 0.5 and 6, so that Π_2 was between 30 and 2.5. An equivalent number is difficult to estimate for geological systems, as a weak inclusion may become invisible after large amounts of shear. If we consider our weak inclusion to represent a crack, whose size may range from micrometers to kilometers, Π_2 may have any value, including those of our experiments.

The viscosities define two dimensionless parameters:

$$\Pi_3 = \frac{\eta_2}{\eta_1} , \text{ and} \tag{3}$$

$$\Pi_4 = \frac{\eta_c}{\eta_1}. \quad (4)$$

In our experiments, Π_3 varied between 1 and 50. In nature, viscosity ratios are strongly dependent on the rock-types and temperature. Schmid et al. (2010) estimated that Π_3 may range from 1 to 10000. Our experiments, therefore, explored the lower range of possible viscosity ratios.

The inclusion was significantly weaker than the weakest silicone that we used, such that $\Pi_4 << 1$. If we take again the weak inclusion to represent a crack, its viscosity should ideally be infinitely weaker than that of its surrounding matrix. In this case, the actual value of Π_4 does not matter, as long as it remains <<1.

The last dimensionless parameter corresponds to the Newton flow law, which links stress, strain rate, and viscosity:

$$\Pi_5 = \frac{\sigma}{\eta \dot{\varepsilon}}. \quad (5)$$

In the experiments, both the viscosity and the strain rate were constant, but we did not control or measure stress. As long as an experimental strain rate remains below the upper limit for viscous deformation of PDMS (5×10^{-1} s^{-1} according to ten Grotenhuis et al., 2002), the silicone behaves like as a Newtonian fluid and Π_5 is 1. This would also be true for ductile rocks if they were Newtonian fluids. However, most ductile rocks obey more complex flow laws, such as non-linear power flow laws. Our experiments are therefore a simplification of geological systems.

We neglect all stresses originating from gravity, as the internal density contrasts and dimensions of the models were small.

	Definition of parameters	Dimensions
a	Inclusion height	m
b	Layer thickness	m
d	Sheath fold depth	m
h	Sheath fold height	m
w	Sheath fold width	m
α	Opening angle	degrees
γ	Strain	
$\dot{\varepsilon}$	Strain rate	s^{-1}
η_1	Viscosity weak silicone	Pa s
η_2	Viscosity strong silicone	Pa s
η_c	Viscosity crack	Pa s
σ	Stress	Pa

Table 2: Viscosity of silicones in this study, measured at room temperature (19-23°C).

3.3. Results

We conducted a test experiment with no inclusion (T) and two series of experiments, each with one inclusion (Figure 5). In the first series with inclusions (V-series) the initial layer thickness was 1 mm and the viscosity ratio between the two silicones was in the range of 1 to 50 (Tab. 2). In the second series with inclusions (L-series), the viscosity ratio was 10 and the layer thickness was in the range of 0.5 mm to 6 mm (Table 2).

We analyzed cross-sections perpendicular to the shear direction. We did not examine cross-sections parallel to the shear direction, as these were technically difficult to obtain. We use the term sheath fold in the following sections for structures that exhibit eye-patterns in cross-sections perpendicular to the shear direction. We are aware that some of these structures may not qualify as sheath folds according to the strict definition of Ramsay and Huber (1987), for which the opening angle should be smaller than 90°.

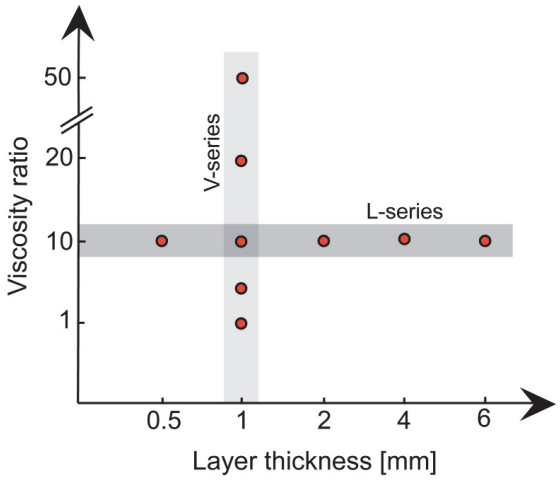

Figure 5: Graph of the experimental strategy. Variables are viscosity ratio and layer thickness.

3.3.1. Experiment T with no inclusion

In this experiment, the model consisted of horizontal layers, 1mm thick. The two silicones were of identical viscosity but different colors (Tab. 2). After deformation (Figure 6), the layers had acquired deflection close to the stationary walls, but not in the center of the model (as in Cobbold and Quinquis, 1980, Figure 11). Small local deflections (white arrows, Figure 6) were due to the rise of air bubbles trapped in the silicone during the preparation procedure.

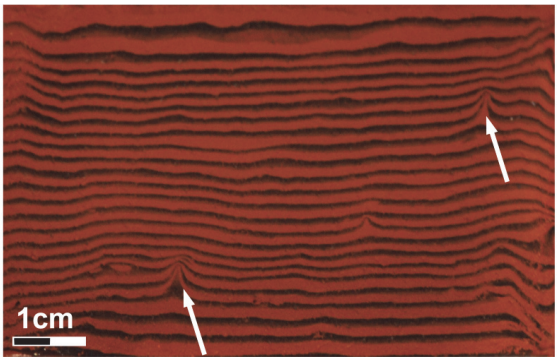

Figure 6: Restored cross-section, test experiment T (layer thickness = 1 mm, viscosity ratio = 1, no inclusion). Section was cut at 2.5 cm from middle of model. Some folds formed within

<1 cm of stationary boundaries (e.g. at right side of photograph). White arrows indicate piercing structures around rising air-bubbles.

3.3.2. Experiments with inclusion

All the models containing inclusions acquired complex deformation patterns. We consider four domains relative to the position of the deformed inclusion, as for the experiment having a layer thickness of 1 mm and a viscosity ratio of 20 (V4; Figure 7). For descriptive purposes, the shear sense is top to the left. The middle of the inclusion is the reference point (0) on a horizontal axis parallel to the shear direction (x-axis). Henceforth, the position of cross-sections will be in cm from the reference point, negative to the left and positive to the right (Figure 7).

Domain 1 is located to the left of the inclusion. A small elliptical shape is visible in the upper right part of the cross-section. This structure indicates the presence of a sheath fold. In all experiments, the sheath folds in domain 1 did not develop well, as they were strongly influenced by the boundaries. Notably, the moving top boundary prevented the sheath fold from developing fully. In addition, the layers in the lower part of the section, next to the sliding plates, deformed strongly.

Domain 2 contains the deformed inclusion (Figure 7). Around it the layers remained approximately horizontal and parallel to the inclusion and no sheath fold was visible.

Domain 3 is located to the right of the inclusion. Here, concentric closed contours reveal fully developed sheath folds (Figure 7). The folds developed close to the middle of the model, so that we infer minimal boundary effects.

Domain 4 is located to the right of domain 3. Here, the layers are almost undisturbed, and no closed contours are visible.

The sheath folds in domains 1 and 3 are not equally well developed, perhaps due to a slight difference in the position of the inclusion. Due to the smaller density of the soap the inclusion tends to be in the upper half of the model. We consider only domain 3 for further analysis.

The opening angles of all the sheath folds developing in domain 3 are smaller than 90° (Figure 12 and 15). According to the definitions of Ramsay and Huber

(1987), Skjernaa (1989), and Marques et al. (2008), our folds are true sheath folds. Some of them would even classify as tubular folds (V1, V2, V3/L2, Skjernaa, 1989).

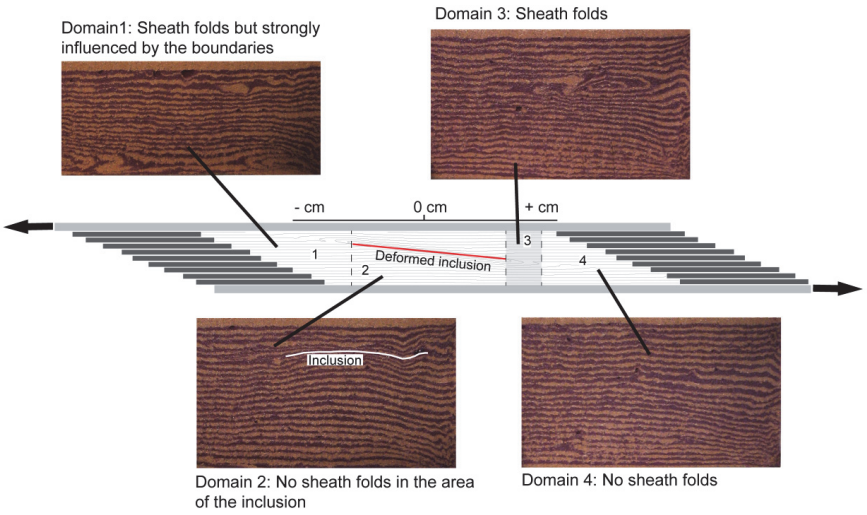

Figure 7: Domains displaying different styles of layer deformation. Red line represents stretched and deformed inclusion, thin black lines represent deformed layers. Middle of inclusion is reference point (0). Restored cross-sections (from experiment V4) represent four domains. Domain 1 contains sheath fold, strongly affected by boundaries (cross-section was at -10 cm from 0). Domain 2 contains deformed inclusion (white line). Cross-section was through 0. Domain 3 shows fully developed sheath fold (cross-section was at 3 cm from 0). In domain 4 no deflection of layers is visible (cross-section was at 10 cm from 0).

3.3.2.1. V-series

The V-series aimed to test the effect of the viscosity ratio. The layer thickness for all the experiments in this series was b = 1 mm (Tab. 2). Figure 8 shows the restored cross-sections of the five experiments. We chose these sections as they represent the characteristic deformation patterns observed in each experiment. In all experiments, we can recognize the three groups of layers defined by Reber et al. (2012, Figure 1): (1) layers, which are remote to the inclusion and show little or no deformation, (2) layers exhibiting omega-like (Ω) shapes, where a central fold separates two straight segments of the layer, and (3) layers forming closed shapes (Figure 8).

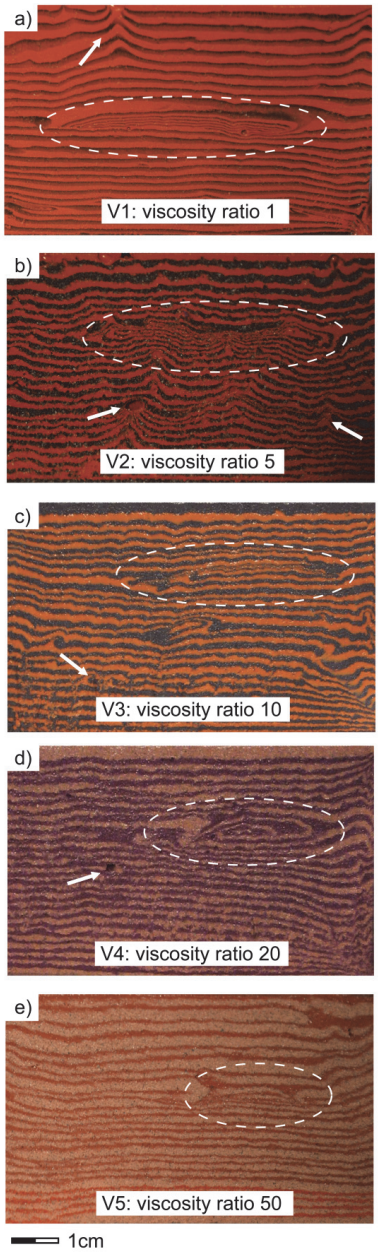

Figure 8: Restored cross-sections, experiments of V-Series (layer thickness = 1 mm). Dashed ellipses highlight area of eye-patterns or strongly folded layers. White arrows indicate air bubbles. a) V1, viscosity ratio = 1, cut at 4.5 cm from 0, b) V2, viscosity ratio = 5, cut at 3

cm from 0, c) V3, viscosity ratio = 10, cut at 4.5 cm from 0, d) V4, viscosity ratio = 20, cut at 5 cm from 0, e) V5, viscosity ratio = 50, cut at 2.5 cm from 0.

In experiment V1 (Figure 8a), the viscosity ratio was 1. In contrast to the test experiment T (Figure 6), experiment V1 shows an eye-structure, *i.e.* a sheath fold. Nine layers partake in the eye-structure while the others are only gently deformed. The layers forming the eye-structure are thinner than the undeformed layers. Deflection of the layers on the right boundary of the picture, due to the stationary boundary wall, is within a 5 mm wide strip. On the left side of the picture, this deflection cannot be seen, as the photograph has been cropped (compare Figure 4). The piercing structure above the sheath fold (white arrow) is due to the rise of a small air bubble. At the bottom of the picture (Figure 8a) the layers are slightly perturbed due to the influence of the sliding plates.

In experiment V2 (Figure 8b), the viscosity ratio was 5. The black colored silicone is the stiffer. The cross-section shows an eye-structure deforming eight layers. It also shows many perturbations and piercing structures due to rising air bubbles. Very little deformation is visible at the right and bottom boundaries.

In experiment V3 (also L2; Figure 8c), the viscosity ratio was 10. The light colored (orange) silicone was the weaker. The eye-structure involves five layers. Below the main eye-structure, a smaller one is visible. This structure was unintentional, as it nucleated from an air bubble. The cross-section shows no other perturbation due to rising bubbles. The wave-like distortion in the unfolded layers (see 5 top layers in Figure 8c) is an artifact of the cutting process. Again, there is some deformation of the layers due to the stationary boundary walls.

In experiment V4 (Figure 8d), we increased the viscosity ratio to 20. The light colored (brown) silicone was the stronger. The eye-structure involved five layers. To the left of the eye-structure a stiff layer is remarkably thickened, in contrast to experiments with smaller viscosity ratios. The deflection of the layers on the right boundary wall is within a very small area. There is also a deflection at the bottom boundary. Some air bubbles are visible, but they were not able to rise through the stiff silicone and did not perturb the layers.

In experiment V5 the viscosity ratio was highest (50; Figure 8e). The light colored silicone (light brown) was the stiffer. Note that the dark and light layers,

where they are horizontal, do not exhibit the same thickness. This is due to the limitation of our technique for producing the thin layering with a high viscosity contrast. The cross-section shows four layers that are strongly folded in the middle of the model where one of the stiff layers shows significant thickening. Very little deformation due to the boundaries and few air bubbles can be observed in the section.

Note that the cross-sections of figure 8 are cut at different locations and that the numbers of the layers in the eye-structures within one experiment is dependent on the distance from the reference point. Therefore, the number of layers in one cross-section is not characteristic of the entire sheath fold.

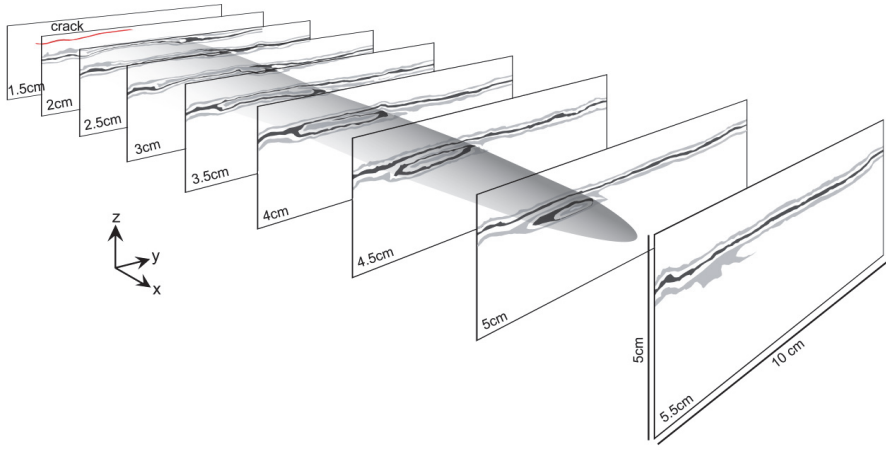

Figure 9: 3D perspective diagram, Experiment V4. In reality, sections are between 1.5 cm and 5.5 cm from 0. For simplicity, only three layers of weak silicone are visible. Red line on section at 1.5 cm is trace of inclusion. Shaded grey area represents approximate shape of sheath fold in black layer. Note that the sketch is exaggerated in x-direction.

The discussed cross-sections give only sparse information concerning the three-dimensional shape of the sheath fold. In figure 9 we show a sketch of a 3D reconstruction of experiment V4 based on the serial cross-sections. This reconstruction was done using the cross-sections of domain 3, in addition to the last section at the right side of domain 2 and the first section to the left of domain 4. The closed contours are not very prominent close to the inclusion and become more

pronounced farther away from the inclusion. In comparison to figure 9 where the sheath fold is sketched with an x-axis that is exaggerated, figure 10 shows an accurate reconstruction of the sheath fold shape. We used a geomodeling software (gOcad, see Appendix B) to interpolate the shape of the sheath fold between the individual slices. The sheath fold in figure 10 shows an opening angle of 53°.

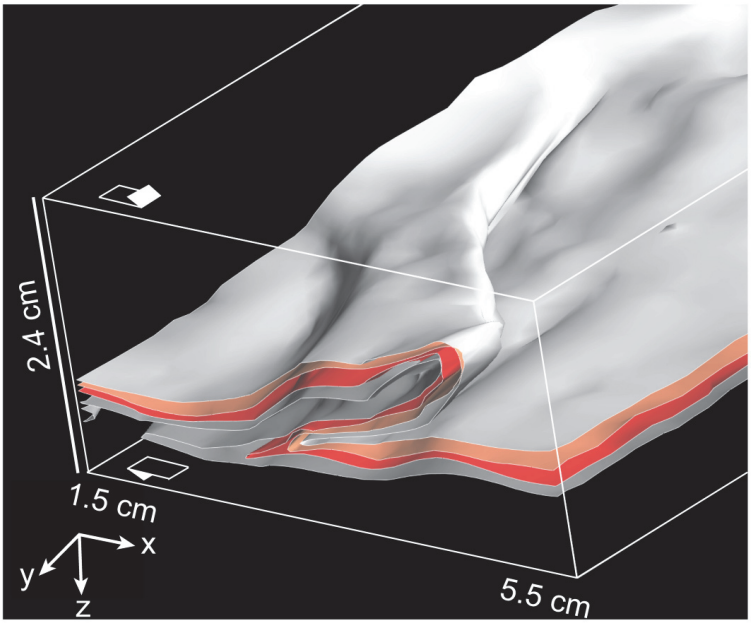

Figure 10: 3D reconstruction of Experiment V4 using gOcad 3D modeler. Four layer interfaces define sheath fold. Arrows indicate shear direction.

To quantify the impact of the viscosity ratio on the shape of the sheath fold, we measured three parameters in each cross-section: *w* (width of the outermost closed contour), *h* (height of the outermost closed contour), and *d* (distance from the upper model boundary to the outermost closed contour).

In all experiments, *w* decreases linearly with increasing *x* (Figure 11a). Linear interpolation of the data provides a slope, which defines the average tangent of the opening angle (α) of the fold. A steeply dipping line corresponds to a bigger opening angle. The opening angle correlates positively with the viscosity ratio (Figure 12a). The error bars show the confidence interval of 95%.

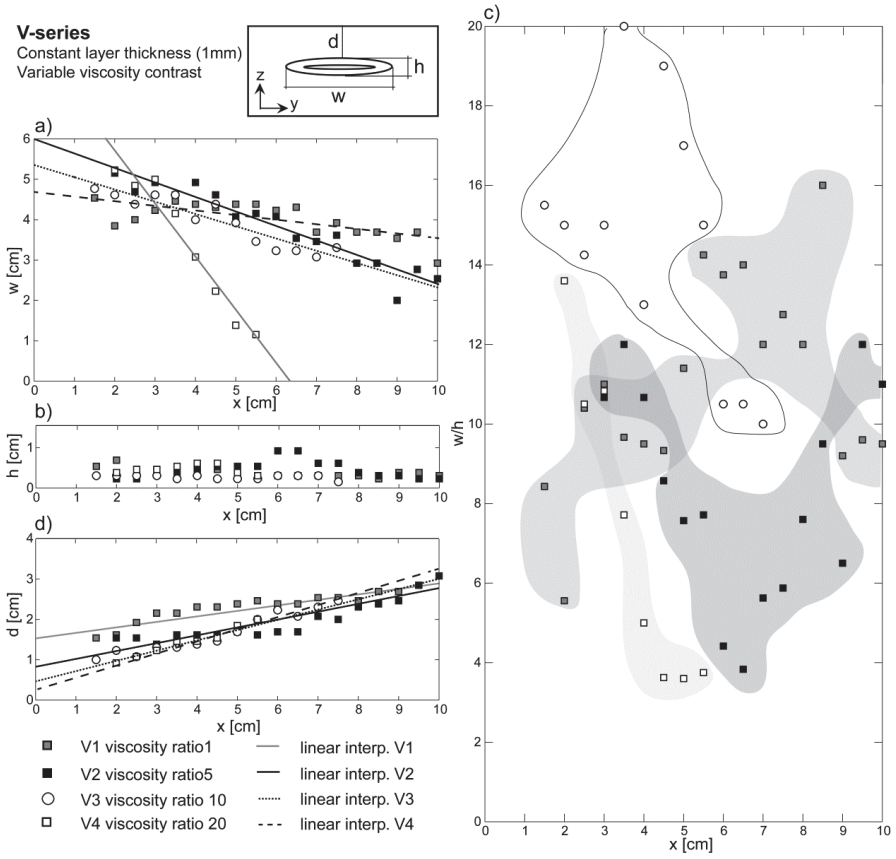

Figure 11: Geometrical parameters versus horizontal distance (x) from reference point (0) for experiments of V-Series. Sketch at top illustrates where the geometrical parameters were measured on serial cross-sections. a) Width of outermost closed contour (w) versus x. b) Height of outermost closed contour (h) versus x. c) Ratio w/h versus x. d) Distance between upper model boundary and outermost closed contour (d) versus against x. Lines represent linear interpolation between data points for four different sheath folds.

The data for V1 and V3 show very little change in *h*, whereas the data for V2 and V4 show an increase followed by a decrease of *h* with increasing *x* (Figure 11 b). Note that the sheath fold height seems to depend neither on *x* nor on the viscosity ratio.

No clear trend in the *w/h* ratio plotted against *x* can be seen for any of the experiments (Figure 11 c). There is no systematic correlation between the

experiments, as the values for V3 are the highest, whereas the values for V4 are among the lowest.

For all experiments, *d* increases approximately linearly with increasing *x* (Figure 11 d). The depths of the sheath folds do not show a clear dependence on the viscosity ratio. The slope of the linear interpolation representing the dip of the folds, however, increases with an increasing viscosity ratio (Figure 12c).

Figure 12b shows the relationship between the viscosity ratio and the sheath fold length. The sheath fold length corresponds to the width of domain 3, as defined in Figure 7. The error bars represent the uncertainty from the measurements. As we cut the model every 5 mm it is possible to underestimate the length of the sheath fold by 10 mm. For experiment V1, the measured length of the sheath fold is even more underestimated, as we could not observed the fold entirely because the construction of the machine prevented a cutting of the model to the point where no closed contours were visible anymore. The length of the sheath fold is negatively correlated to the viscosity ratio (Figure 12b).

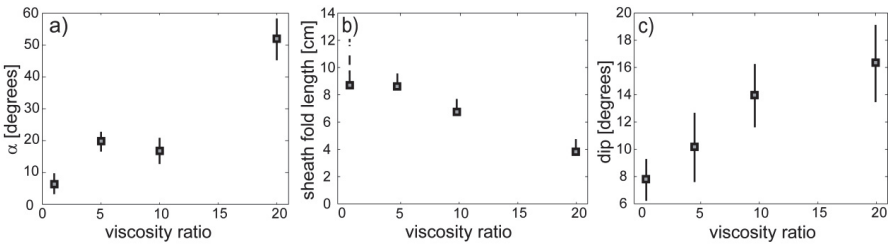

Figure 12: Plots showing dependence of a) opening angle, b) length, and c) dip on horizontal distance (x), for sheath folds of V-Series. Error bars for a and c correspond to 95% confidence intervals.

3.3.2.2. L-series

The L-series aimed to test the impact of the layer thickness on the sheath fold development. The viscosity ratio for all experiments was 10 while we varied the layer thickness from 0.5 mm to 6 mm. Similarly to the V-series, we chose the cross-sections as they represent the characteristic deformation patterns in each experiment (Figure 13).

In experiment L1 (Figure 13a), the layer thickness was 0.5 mm. The light colored (red) silicone was the weaker. The very thin individual layers were rather hard to track, as they were in some places discontinuous. In the upper third of the photograph, strongly deflected layers are visible (dashed ellipse); several of them display eye-patterns. Some of the layers show thickening at the vicinity of the eye-structure. A number of air bubbles locally dislocated the layers. The deflection at the boundaries is minor.

In experiment L2 (also V3, Figure 13b) the layer thickness was 1 mm. Here we show a different cross-section than the one described for the V-series (Figure 8c). A major eye-structure involves seven layers. A smaller eye-structure was the result of an air bubble and unintended. Gentle deflections of the layers can be seen at the right boundary. The wave-like deformation of the layers is an artifact of the cutting.

In experiment L3 (Figure 13c), the layer thickness was 2 mm. In this cross-section, two layers are strongly deformed but the eye-pattern cannot unambiguously be observed. It is possible that a small sheath fold developed but that we did not sample it with the cores cross-section spacing of 5 mm. Some deflections of the layers due to the cutting can be observed in the lower right corner. Otherwise, the layers are only slightly distorted at the boundaries. The section shows many air bubbles, but they have small effect, as they did not rise through the stiff silicone.

In experiment L4 (Figure 13d) the layer thickness was 4 mm. This cross-section is very similar to the one from experiment L3. Two layers are strongly deformed, but they show no eye-pattern. Again, the influences of the boundary walls and the air bubbles are minimal.

In experiment L5 (Figure 13e), the layer thickness was 6 mm. The eye-pattern involves one layer. This cross-section is the only one in the entire experiment showing such a closed feature. The deformation patterns in the other cross-sections of L5 are similar to those of experiment L4. The boundaries and the bubbles have nearly no effect.

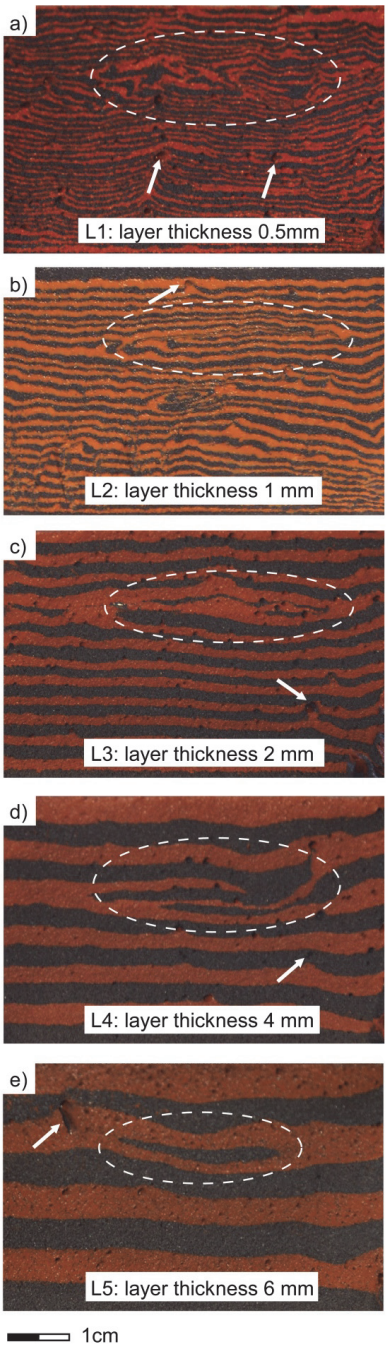

Figure 13: Restored cross-sections from experiments of L-Series. Viscosity ratio has constant value of 10. Dashed ellipses highlight area of eye-patterns or strongly folded layers.

White arrows indicate air bubbles. a) Experiment L1, layer thickness = 0.5 mm, cut at 5.5 cm from 0, b) Experiment L2, layer thickness = 1 mm, cut at 4 cm from 0, c) Experiment L3, layer thickness 2 mm, cut at 4 cm from 0, d) Experiment L4, layer thickness = 2 mm, cut at 5 cm from 0, e) Experiment L5, layer thickness 6 mm, cut at 5 cm from 0.

Similarly to the V-series, we measured *w*, *h*, and *d*, and plotted them against the horizontal distance *x* (Figure 14). Experiment L4 was not considered in any of these measurements, as it showed no closed contour and could therefore not unambiguously be identified as a sheath fold. For experiment L5 only one cross-section shows a closed contour. Thus, only one point represents experiment L5 in the plots of figure 14.

For the experiments L2 and L3, *w* decreases with increasing *x* (Figure 14a). In contrast, *w* increases with increasing *x* for experiment L1. The lines represent the linear interpolations of the data points for each experiment and give the tangent of the opening angles (α) of the folds (Figure15a). The error bars are calculated for a confidence interval of 95%. The fit for experiment L1 is poor due to the big uncertainty for detecting the closed contours in the cross-sections. The resulting slope for L1 is positive, which means that the width of the fold increases away from the inclusion. We consider this result to be meaningless. Not enough experiments were conducted to conclude that the width of the sheath fold and the opening angle depend on the layer thickness (Figure 15a).

The *h* values of all three experiments are close to each other and show little dependence on *x* or the layer thickness (Figure 14b).

Figure 14c displays the *w/h* ratio against *x*. No clear pattern can be observed in this plot.

In all three experiments, *d* shows a positive linear correlation with *x* (Figure 14d). All the data points plot close to each other. The dip of the sheath fold corresponds to the slope of the linear interpolation of the data. The error bars are calculated for a confidence interval of 95% (Figure 15c). The error bars are too large to allow for a correlation between the dip angle and the layer thickness.

The lengths of the sheath folds show no consistent correlation with the layer thickness (Figure 15b). In experiment L1, however, the sheath fold length must be substantially underestimated due the difficulty to detect closed contours. The error

bar represents again the uncertainty of the length of the sheath fold because of the spacing of the cross-sections.

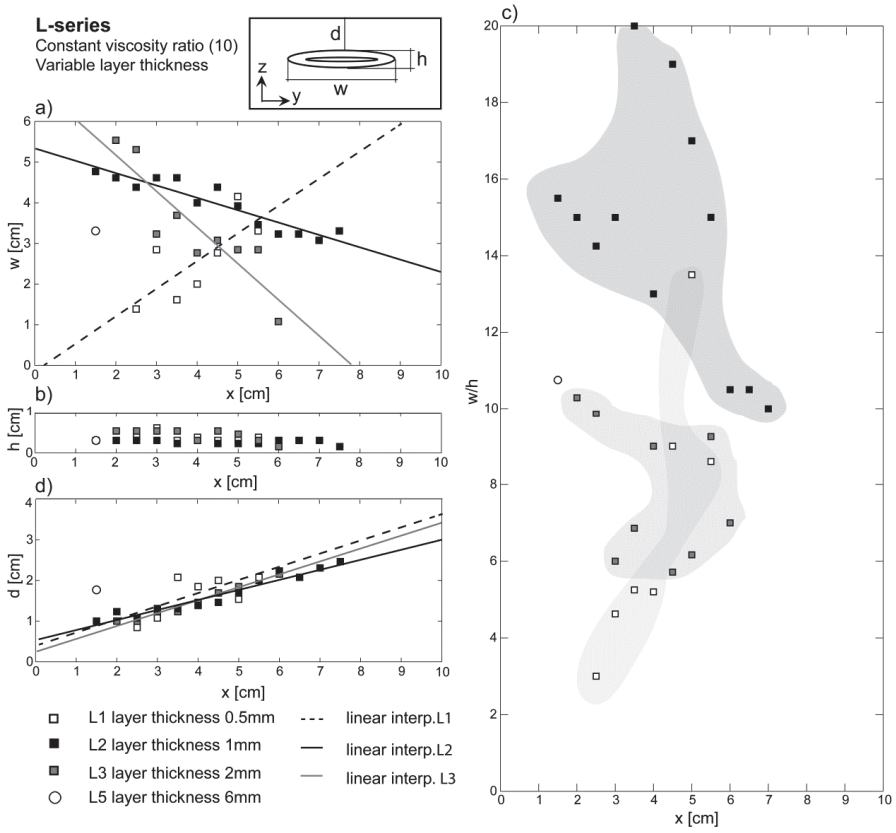

Figure 14: Geometrical parameters versus horizontal distance x from reference point (0) for experiments of L-Series. Sketch at top illustrates where geometrical parameters were measured in serial cross-sections. a) Width of outermost closed contour (w) versus x. b) Height of outermost closed contour (h) versus x. c) Ratio w/h versus x. d) Distance between upper model boundary and outermost closed contour (d) versus x. Lines represent linear interpolation between data points for three different sheath folds. Note that there are no data points for experiment L4 (layer thickness 4 mm) as in this experiment we detected no sheath fold.

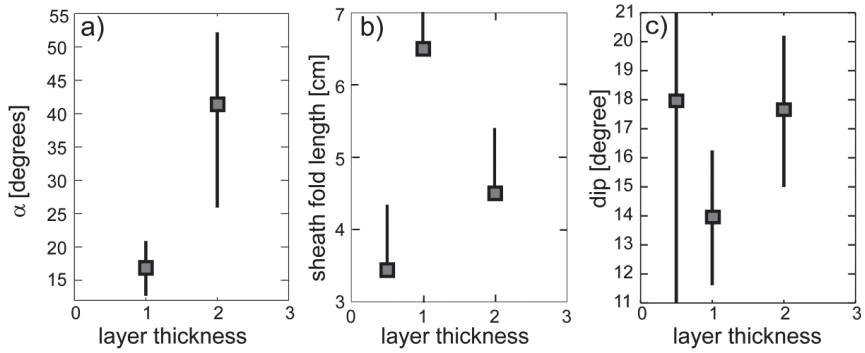

Figure 15: Plots showing a) opening angle, b) length, c) dip of sheath folds from L-series versus x.

3.4. Discussion

3.4.1. Validity of experimental method

The amount of applied shear strain ($\gamma = 6$) requires a relatively small model, which can lead to substantial influence of the boundaries on the structures. To minimize the boundary effects of the vertical, stationary, shear parallel sidewalls (x-z plane), we lubricated them with liquid soap. The soap is 8800 times weaker than the weakest silicone we used. For normal stresses that are not large enough to cause extrusion, Cobbold (1973) showed that such liquid soap is a good lubricating agent, able to reduce boundary effects on the sidewalls. Indeed, in our experiments, boundary effects were visible only within a few millimetres of the stationary walls (see Figure 7 right edge of the model). Cobbold and Quinquis (1980) discussed such boundary effects and illustrated them for a model in which there was no lubrication of the stationary walls. Using two-dimensional numerical calculations, Frehner et al. (2011) showed that the viscous drag of a lubricating fluid can perturb a model, but they did not consider the stabilizing influence of a model that is relatively wide in the y-direction. Also, in the calculations of Frehner et al. (2011), the viscosity ratio between model and lubricant was 100:1, in other words, almost two orders of magnitude smaller than the viscosity ratio in our experiments. We thus infer that the boundary effect, due to the lubricating fluid, was much higher in their simulations than in our models. In contrast, the sliding plates of the simple shear machine

produce substantial boundary effects. In our experiments, these effects concentrated close to the sliding plates, leaving an unperturbed area of more than 10 cm length in the middle of the model (Figure 7). The sheath folds we observed and analyzed developed in this area. The horizontal boundaries (x-y plane), *i.e.* the horizontal moving plates, transmit the shear stress that drives the deformation and confine the model in the y-direction. In our experiments, the silicone adhered to these moving plates and we observed no corresponding boundary effects.

Because the centre of the model was in principle a centre of symmetry, we might have expected two sheath folds to form, one at the lower tip of the inclusion and the other at its upper tip. In our experiments, however, a sheath fold developed strongly at the lower tip, but another developed not so strongly at the upper tip. We attribute this asymmetry to a slight offset of the inclusion, with respect to the centre of the model. Because the density of the inclusion was smaller than that of the silicone matrix, the inclusion tended to rise.

Constraining the viscosity of the silicone layers is essential for experiments such as ours. The viscosity of the silicone is dependent, not only on the amount of inert fillers or oil, but also on the temperature. We therefore measured the viscosity of each batch of silicone, just before using it. Although the viscosities of the silicones changed slightly, from one experiment to another, the viscosity ratios were identical (Tab. 2).

By adding sand, iron-oxide or oil to the silicone we induced a change in the overall density. The density contrast between the individual layers, however, was too small to trigger gravitational instabilities in the time frame of the experiment. We infer that the density ratio had a negligible effect in the models.

Another problem in experiments on silicone is the presence of air bubbles. To reduce them, we let each batch of silicone rest for at least a day after preparing it. However, the technique that we adopted for preparing multilayers introduced small bubbles, which later acted as weak inclusions. When the bubbles were large enough, small sheath folds formed around them (Figure 8b and Figure 13b; see also Marques et al., 2008, their Figure 7a). Another source of air in the model was the insertion of the inclusion.

A process that further disturbed the internal shape of the model was cutting. We systematically restored the sections, but cannot be entirely sure that they were thus faithful to the original ones. Nevertheless, after restoration, the layers away from the sheath folds became almost perfectly horizontal, as one would expect. This gave us confidence in correlating the structures from one cross section to another.

To test for reproducibility, we repeated experiment V1 three times, obtaining almost identical results.

3.4.2. Experimental results

All experiments with an inclusion showed either a sheath fold or a very strong deformation of the layers. In contrast, the test experiment T, with no inclusion, showed no distortion of the horizontal layering. We thus conclude that the inclusion did nucleate the sheath folds.

The correlation between the geometrical characteristics of the sheath folds and the viscosity ratio (Figure 12) shows that this ratio is an important controlling parameter. An increase of the viscosity ratio leads to shorter sheath folds with a larger opening angle. This suggests that an increasing viscosity ratio limits the elongation of sheath folds. An increase of the viscosity ratio also leads to an increase in dip of the sheath folds. This result is somewhat surprising, as former studies showed that the dip and elongation of a passive marker, such as an inclusion or a dyke, depend only on the amount of strain (e.g., Exner and Dabrowski, 2010; Sassier et al., 2009). Hugon (1982) showed that the viscosity ratio between layers undergoing simple shear has an impact on the evolving structures. Our results are in accordance with this and show that the viscosity ratio plays an active role in the development of sheath folds. It suggests, however, that sheath folds do not develop purely passively and that the amount of strain is not the only controlling parameters for their three-dimensional final shape. Our experiments show that the eye-patterns in cross-sections look similar independently of the viscosity ratio between the layers. The existence of a sheath fold is, therefore, not a good criterion for constraining the viscosity ratio in rocks.

The results from the L-series show that the ratio of the inclusion height to layer thickness (Π_2), is a critical factor for the visibility of the sheath folds. When the

layer thickness is ≥ 2 mm (*i.e.* $\Pi_2 \leq 7.5$; experiments L3, L4, L5), it becomes increasingly difficult to observe eye-structures due to low resolution (see Dabrowski and Schmid, 2011). The insufficient resolution leads to strong scattering of the measurements of the height, width and depth of the folds (Figure 14). Although no eye-structure is visible for $\Pi_2 \leq 7.5$, the inclusion has a major impact on the deformation of the layers (Figure 12c, d, e). When the layer thickness is 0.5 mm (i.e. $\Pi_2 = 30$; experiment L1), it is difficult to detect eye-structures because the individual layers are too thin. Nevertheless, we argue that eye-structures formed.

In the V-series, sheath folds formed at a viscosity ratio of up to 20. This result contrasts with those of Marques et al. (2008), who concluded that the viscosity ratio in the matrix has to be lower than 10 to produce a sheath fold around a rigid inclusion. The major difference between their experiments and ours, in addition to the nature of the inclusion, is the layer thickness. We showed in section 3.2.2 that the layer thickness, and overall Π_2, is a critical parameter for the visibility of a sheath fold. In the experiments of Marques et al. (2008) is $\Pi_2 \approx 3.25$. This value is significantly lower than the critical value of 7.5 required for proper observation of sheath folds. The lack of visible sheath folds in the experiments of Marques et al. (2008) is probably due to poor resolution, but it does not imply that no sheath fold formed.

The aspect ratio *w/h* shows no correlation with *x*, with viscosity ratio or with layer thickness. This observation questions the usefulness of aspect ratios of closed contours as a tool for sheath fold classification (Alsop and Holdsworth, 2006).

3.4.3. Implications

There are striking similarities between our experimental results and natural examples of sheath folds (Figure 16). Sheath folds from Oppdal, Norway (Figure 16a) and Cap de Creus, Spain (Figure 16b) have the three groups of layers defined by Reber et al. (2012), including the closed contours and the omega-like layers (for example the dominant light colored layer in Figure 16a). Notice that in Figure 16b the light-colored layer to the right of the eye structure experienced thickening. Our experimental results show very similar features (Figure 16c and d). They reproduce the first-order observations of the natural sheath folds.

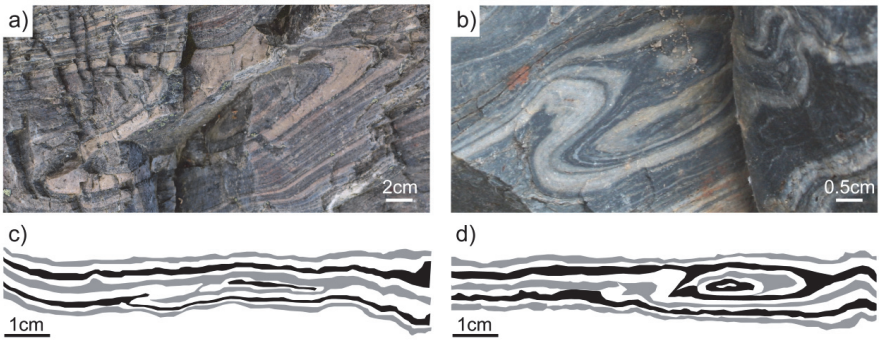

Figure 16: a) Photograph of sheath fold in layered quartzite in section perpendicular to stretching direction, Oppdal, Norway. b) Photograph of sheath fold cut perpendicular to shear direction, Cap de Creus, Spain. c) Sketch of reconstructed section of experiment V3/L2 cut at 5 cm from 0. Only a selected number of weak layers are highlighted. d) Sketch of reconstructed section of experiment V4 cut at 5 cm from 0. Again, only some of the weak layers are shown.

With our current knowledge, we cannot estimate the viscosity ratio between layers in natural examples. But as the color difference of the layers comes along with a change in mineral composition, it is unlikely that the folds formed in a homogeneous matrix. Even though we varied the viscosity ratios in the experiments of the V-series, the eye-structures on the cross-sections show the same features and no systematic difference. Therefore, on the basis of 2-dimensional observations only, we could not detect a feature that is characteristic of the viscosity contrast, either in nature or in our experiments. In contrast, the results from the V-series experiments show that the whole 3-dimensional shape of the sheath folds needs to be considered to infer the viscosity ratio of the matrix.

In our experiments, we did not observe a deformed inclusion (domain 2; Figure 7) and an associated sheath fold (domain 3) on the same cross-section. Two-dimensional observations were thus insufficient to determine why sheath folds formed. An additional problem was that the inclusion deformed and stretched during deformation, becoming difficult to observe. In nature, we expect that identifying the reason for the formation of a sheath fold would be even harder, because the structure may completely detach from its nucleating inclusion. Nevertheless, weak inclusions, such as veins, rheologically weak finite layers, or even cracks, are very common in

all rock types and at all scales. From our results and those of Reber et al. (2012), we infer that weak inclusions are very proficient nucleation features for sheath folds. This mechanism is thus an alternative one to those proposed by e.g., Cobbold and Quinquis (1980) and Marques and Cobbold (1995).

3.5. Conclusion

We tested the effect of a mechanically layered matrix on the development of sheath folds, by varying the viscosity ratio between layers and the layer thickness. Our procedure allows for 3-dimensional reconstruction of the structures. From our results we draw the following conclusions:

- A weak inclusion in a mechanically layered matrix subject to simple shear causes sheath folds to nucleate and develop at both tips of the deformed inclusion.
- The experiments produced sheath folds for viscosity ratios up to 20. For a viscosity ratio of 50, we could not identify closed contours unambiguously, although the layers deformed strongly.
- The viscosity ratio controls the 3D shape of the sheath folds: the dip increases, the fold becomes shorter, and the opening angle widens for a larger viscosity ratio. In contrast, 2D observations (cross sections) are not sufficient to identify a systematic difference for different viscosity ratios.
- The ratio between the inclusion height and the layer thickness (Π_2) greatly influences the visibility of the sheath fold. When $\Pi_2 \leq 7.5$, we did not observe closed contours, although the layers deformed strongly.
- The experimental sheath folds capture the first-order observations from natural sheath folds.
- We expect that the mechanism of sheath fold nucleation from a weak inclusion is common in nature.

Acknowledgements

This work was supported by a Center of Excellence grant from the Norwegian Research Council to PGP. Special thanks go to Jean-Jacques Kermarrec and Mélanie Noury for excellent support in the laboratory and stimulating

discussions. Thanks also go to the Master Students 2011 of Géosciences Rennes, University of Rennes 1 and to Christoph Vettiger for lending a helping hand in the laboratory.

3.6. Appendix A: Viscosimetry

To measure the viscosity we used a concentric-cylinder viscometer (built in the laboratory of Géosciences Rennes, Figure 17a). The setup consists of a fixed outer cylinder and a rotating inner cylinder (Figure 17b). We filled the space between the two co-axial cylinders with silicone. The pull of a weight (200 g) attached to a turning wheel applies a torque to the inner cylinder, which drags the surrounding silicone. We measured the time Δt (s) needed for one rotation of the inner cylinder with a manual stopwatch to calculate the viscosity η (Pa s) from the following equation:

$$\eta = \frac{\Delta t}{2\pi k} \frac{m g r_0}{2\pi l} \frac{1}{2} \left(\frac{1}{r_2^2} - \frac{1}{r_1^2} \right). \quad \text{(A.1)}$$

Here k (non-dimensional) is the number of rotations (here 1), r_0 (meters) is the radius of the turning wheel, r_1 (meters) is the radius of the inner cylinder, r_2 (meters) is the radius of the outer cylinder (see Figure 17), m (g) is the mass of the pulling weight and l (meters) is the height of the outer cylinder.

To determine whether the silicone was a Newtonian fluid, we scratched a straight marker line on the silicone surface between the inner and the outer cylinder. The line deformed, as the inner cylinder rotated, entraining the silicone (Figure 17a). We compared the shape of the deformed line with a set of reference lines (Battegay, 1984) to obtain the exponent of the power-law relationship between stress and strain-rate. For all silicones in this study, power-law exponents were close to 1 (compare Figure 17a with Figure 17c), demonstrating that the silicones behaved as Newtonian fluids. The viscosity measurements (see Tab. 2), resulted in values between 7.2×10^3 Pa s and 5.3×10^5 Pa s at room temperature.

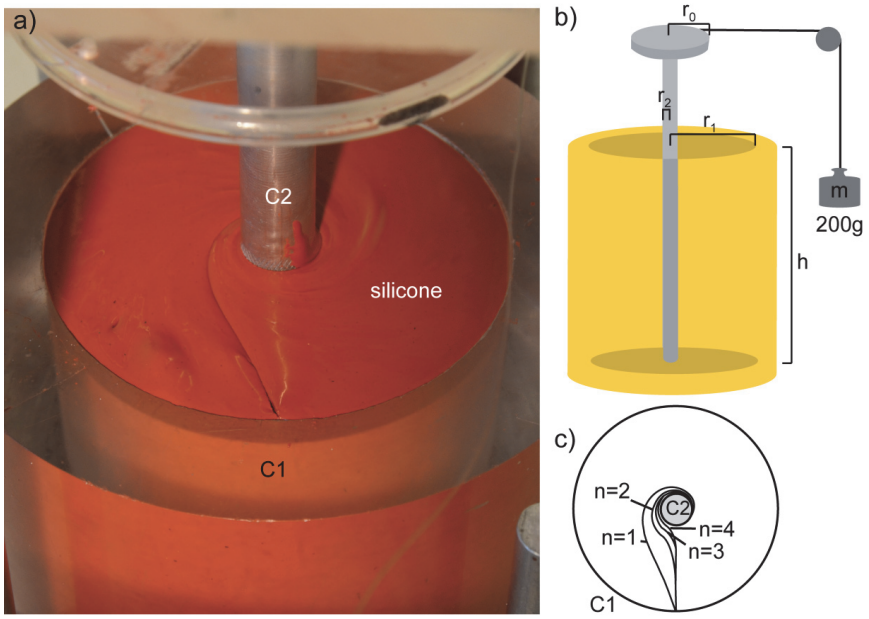

Figure 17: a) Photograph of concentric-cylinder viscometer after one rotation of C2. Line on surface of silicone constrains power-law exponent. b) Sketch of viscometer. Height (l) of cylinder is 0.1 m, $r_0 = 0.05$ m, $r_1 = 0.05$ m, $r_2 = 0.008$ m. c) Reference curves for determining power-law exponent n (Battegay, 1984).

3.7. Appendix B: 3D modeling

We used the gOcad 3D geomodeler (Mallet, 2002) to reconstruct the folds from cross-sections. This modeler allows a discrete representation of geological objects through regular (grid) or irregular meshes (polygonal curves, triangulated surfaces, and tetrahedralised solids; Mallet, 2002). Triangulated surfaces appeared to be particularly relevant for modeling multivalued and/or closed interfaces, such as those observed in sheath folds. The 3D reconstruction of geological structures from the data is based on the Discrete Smooth Interpolation method (DSI, Mallet, 2002). Globally, the construction of the model comprised two main stages:

1. The first step consists of the introduction of cross-sections and the definition of the correlations between these cross-sections. The modeler was particularly useful for checking the 3D consistency of the correlations.

2. In the second stage, triangulated surfaces representing layer interfaces constrained by the cross-sections were built using the DSI method (Mallet, 2002, see also an example of such construction in Le Carlier de Veslud et al., 2009). At the end of this stage, a quality check was performed, especially in order to detect and correct possible interface crossings.

The construction of the surface model using the DSI method provides triangulated surfaces with good-quality meshes (limiting numerical instabilities), which honor data and are geometrically consistent (Caumon et al., 2009).

3.8. References

Alsop, G. I., and Carreras, J., 2007, The structural evolution of sheath folds: A case study from Cap de Creus: Journal of Structural Geology, v. 29, no. 12, p. 1915-1930.

Alsop, G. I., and Holdsworth, R. E., 2004, Shear zone folds: records of flow perturbation or structural inheritance?: Flow Processes in Faults and Shear Zones, v. 224, p. 177-199.

Alsop, G. I., and Holdsworth, R. E., 2006, Sheath folds as discriminators of bulk strain type: Journal of Structural Geology, v. 28, no. 9, p. 1588-1606.

Alsop, G. I., Holdsworth, R. E., and McCaffrey, K. J. W., 2007, Scale invariant sheath folds in salt, sediments and shear zones: Journal of Structural Geology, v. 29, p. 1585-1604.

Balk, R., 1953, Salt structure of Jefferson Island salt dome, Iberia and Vermillion parishes, Louisiana: American Association of Petroleum Geologists Bulletin, v. 37, no. 11, p. 2455-2474.

Barenblatt, G. I., 2003, Scaling: Cambridge, Cambridge University Press.

Battegay, G., 1984, Mise au point d'une technique de viscométrie d'un materiau analoque (silicone) utilisé en modélisation experimental: Diplome d'Etudes Approfondies, Universite de Paris XI.

Berlenbach, J. W., and Roering, C., 1992, Sheath-fold-like structures in pseudotachelytes: Journal of Structural Geology, v. 14, no. 7, p. 847-856.

Biot, M. A., 1957, Folding instability of a layered viscoelastic medium under compression: Proceedings of the Royal Society of London Series A-Mathematical and Physical Sciences, v. 242, no. 1231, p. 444-454.

Branney, M. J., Barry, T. L., and Godchaux, M., 2004, Sheathfolds in rheomorphic ignimbrites: Bulletin of Volcanology, v. 66, no. 6, p. 485-491.

Carreras, J., Estrada, A., and White, S., 1977, Effects of folding on c-axis fabrics of a quartz mylonite: Tectonophysics, v. 39, no. 1-3, p. 3-24.

Caumon, G., Collon-Drouaillet, P., de Veslud, C. L. C., Viseur, S., and Sausse, J., 2009, Surface-Based 3D Modeling of Geological Structures: Mathematical Geosciences, v. 41, no. 8, p. 927-945.

Cobbold, P. R., 1973, Initiation and development of folds in rocks: PhD thesis, University of London, UK, 194 pp.

Cobbold, P. R., and Quinquis, H., 1980, Development of sheath folds in shear regimes: Journal of Structural Geology, v. 2, no. 1-2, p. 119-126.

Dabrowski, M., and Schmid, D. W., 2011, A rigid circular inclusion in an anisotropic host subject to simple shear: Journal of Structural Geology, v. 33, no. 7, p. 1169-1177.

Dixon, J. M., and Summers, J. M., 1985, Recent developments in centrifuge modeling of the tectonic processes- Equiplent, model construction techniques and rheology of model meterials: Journal of Structural Geology, v. 7, no. 1, p. 83-102.

Exner, U., and Dabrowski, M., 2010, Monoclinic and triclinic 3D flanking structures around elliptical cracks: Journal of Structural Geology, v. 32, no. 12, p. 2009-2021.

Ez, V., 2000, When shearing is a cause of folding: Earth-Science Reviews, v. 51, no. 1-4, p. 155-172.

Fossen, H., and Rykkelid, E., 1990, Shear zone structures in the Oygarden area, west Norway: Tectonophysics, v. 174, no. 3-4, p. 385-397.

Frehner, M., Exner, U., Mancktelow, N. S., and Grujic, D., 2011, The not-so-simple effects of boundary conditions on models of simple shear: Geology, v. 39, no. 8, p. 719-722.

Galland, O., Cobbold, P. R., Hallot, E., d'Ars, J. D., and Delavaud, G., 2006, Use of vegetable oil and silica powder for scale modelling of magmatic intrusion in a deforming brittle crust: Earth and Planetary Science Letters, v. 243, no. 3-4, p. 786-804.

George, A. D., 1990, Deformation processes in an accretionary prism- A study from the Torlesse Terrane of New-Zealand: Journal of Structural Geology, v. 12, no. 5-6, p. 747-759.

Hansen, E., 1971, Strain facies, Springer-Verlag.

Hugon, H., 1982, Structures et déformation du Massif de Rocroi (Ardennes): PhD thesis, University of Rennes 1, France.

Lacassin, R., and Mattauer, M., 1985, Kilometer-scale sheath fold at Mattmark and implications for transport direction in the Alps: Nature, v. 315, no. 6022, p. 739-742.

Le Carlier de Veslud, C., Cuney, M., Lorilleux, G., Royer, J.-J., and Jébrak, M., 2009, 3D modeling of uranium-bearing solution-collapse breccias in Proterozoic sandstones (Athabasca Basin, Canada)—Metallogenic interpretations: Computers & Geosciences, v. 35, no. 1, p. 92-107.

Mallet, J. L., 2002, Geomodeling. Applied Geostatistics, New York, Oxford University Press.

Mandal, N., Mitra, A. K., Sarkar, S., and Chakraborty, C., 2009, Numerical estimation of the initial hinge-line irregularity required for the development of sheath folds: A pure shear model: Journal of Structural Geology, v. 31, no. 10, p. 1161-1173.

Marques, F. G., and Cobbold, P. R., 1995, Development of highly noncylindrical folds around rigid ellipsoidal inclusions in bulk simple shear regimes - Natural examples and experimental modeling: Journal of Structural Geology, v. 17, no. 4, p. 589-602.

Marques, F. O., Guerreiro, S. M., and Fernandes, A. R., 2008, Sheath fold development with viscosity contrast: Analogue experiments in bulk simple shear: Journal of Structural Geology, v. 30, no. 11, p. 1348-1353.

McClelland, H. L. O., Woodcock, N. H., and Gladstone, C., 2011, Eye and sheath folds in turbidite convolute lamination: Aberystwyth Grits Group, Wales: Journal of Structural Geology, v. 33, no. 7, p. 1140-1147.

Minnigh, L. D., 1979, Structural-analysis of sheath-fold in meta-chert from the Western Italian Alps: Journal of Structural Geology, v. 1, no. 4, p. 275-282.

Morales, L. F. G., Casey, M., Lloyd, G. E., and Williams, D. M., 2011, Kinematic and temporal relationships between parallel fold hinge lines and stretching lineations: A microstructural and crystallographic preferred orientation approach: Tectonophysics, v. 503, no. 3-4, p. 207-221.

Nicholson, R., 1963, Eyed folds and interference patterns in the Sokumfjell marble group, northern Norway: Geol. Mag., v. 100, p. 59-70.

Philippon, M., Brun, J. P., and Gueydan, F., 2009, Kinematic records of subduction and exhumation in the Ile de Groix blueschists (Hercynian belt; Western France): Journal of Structural Geology, v. 31, no. 11, p. 1308-1321.

Quinquis, H., Audren, C., Brun, J. P., and Cobbold, P. R., 1978, Intense progressive shear in Ile de Groix bluschists and compatibility with subduction or obduction: Nature, v. 273, no. 5657, p. 43-45.

Ramsay, J. G., 1980, Shear zone geometry - A review: Journal of Structural Geology, v. 2, no. 1-2, p. 83-99.

Ramsay, J. G., and Huber, M. J., 1987, The techniques of modern structural geology. Volume 2: Folds and fractures, Academic Press, London.

Reber, J. E., Dabrowski, M., and Schmid, D. W., 2012, Sheath fold formation around slip surfaces: Terra Nova, v. 24, p. 417-421.

Rosas, F., Marques, F. O., Luz, A., and Coelho, S., 2002, Sheath folds formed by drag induced by rotation of rigid inclusions in viscous simple shear flow: nature and experiment: Journal of Structural Geology, v. 24, no. 1, p. 45-55.

Sassier, C., Leloup, P. H., Rubatto, D., Galland, O., Yue, Y., and Lin, D., 2009, Direct measurement of strain rates in ductile shear zones: A new method based on syntectonic dikes: Journal of Geophysical Research-Solid Earth, v. 114.

Schmid, D. W., Schmalholz, S. M., Mancktelow, N. S., and Fletcher, R. C., 2010, Comment on 'Folding with thermal-mechanical feedback': Journal of Structural Geology, v. 32, no. 1, p. 127-130.

Skjernaa, L., 1989, Tubular folds and sheath folds - Definitions and conceptual models for their development, with examples from the Grapesvare Area, Northern Sweden: Journal of Structural Geology, v. 11, no. 6, p. 689-703.

ten Grotenhuis, S. M., Piazolo, S., Pakula, T., Passchier, C. W., and Bons, P. D., 2002, Are polymers suitable rock analogs?: Tectonophysics, v. 350, p. 35-47.

Weijermars, R., 1986, Flow behaviour and physical chemistry of bouncing putties and related polymers in view of tectonic laboratory applications: Tectonophysics, v. 124, p. 325-358.

5. Shear plane parallel cross-sections

5.1. Introduction

The last three chapters showed that sheath folds develop readily from weak inclusions. This leads to the evident question: why do we not observe more sheath folds in nature? Assuming that weaknesses, able to act as slip surfaces, are widespread in nature, it is surprising that sheath folds are not recorded more often. A possible answer to this question is that we do not recognize sheath folds as such if they are exposed in outcrops that are not perpendicular to the stretching direction. As already shown in chapter 2, sheath folds show great similarity to flanking folds (Passchier, 2001) when they are cut parallel to the stretching direction. Exner and Dabrowski (2010) suggested that sheath folds are possibly flanking structures exposed in three dimensions. Conversely, we could say that some flanking structures are sheath folds that are cut parallel to the stretching direction.

Based on the characteristic eye-pattern, we recognize sheath folds in cross-sections perpendicular to the stretching direction. However, this cross-section orientation is very specific. Considering sheath folds in shear zones (e.g., Alsop and Carreras, 2007) where the folds are elongated in the shear direction, we would also expect cross-sections that are parallel to the shear direction. In this chapter, we investigate the patterns on cross-sections parallel or with a small angle to the shear plane.

5.2. Method

The sheath fold used for this analysis is modeled with the same analytical solution as presented in chapters 2 and 4. The initial orientation of the slip surface is $\theta = 90°$ and its aspect ratio $a/b = 2.67$. The sheath fold is sheared to a strain of $\gamma = 6$. For the three dimensional visualization, we use ParaView. We visualize the sheath

fold in such a way that the top layer shows the cone shape (Figure 1a, green layer). We cut the sheath fold at different angles (α) with respect to the shear plane (Figure 1b) and vary the depth of the cutting plane in z-direction.

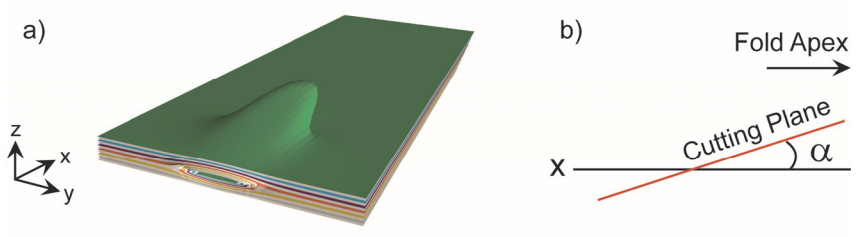

Figure 1: a) Initial sheath fold. b) The cutting plane is tilted with an angle α with respect to the horizontal shear plane.

5.3. Results

We investigated patterns in cross-sections parallel or with a small angle to the shear plane. We used α values of -6, -3, 0, 3, and 6 degrees with respect to the shear plane (Figure 2). The cutting plane is inclined towards the apex of the fold for α = 3 and α = 6. For negative α the cutting plane is inclined towards the center of the fold structure. Cross-sections with α = 0 are parallel to the shear plane. We varied the depth of the crosscutting plane in z–direction. Cross-sections cut only through the cone of the fold (first two figures in each column in Figure 2) reveal several closed contours nested in each other for all α orientations. These cross-sections look similar to cross-sections perpendicular to the shear direction. The center of the eye-structure is located towards the apex of the fold. When the cross-section plane is moved downwards in z-direction, the patterns get more complex and larger differences are visible for the different α orientations. For α = -6 (Figure 2a), closed contours together with ’folded’ layers are observable. For the two cross-sections that cut the structure below the actual cone, only ‘folded’ layers are visible.

Figure 2: Cross-sections cut through a sheath fold (θ = 90, a/b = 2.67, γ = 6) at an angle α with respect to the shear plane. a) α = -6, b) α = -3, c) α = 0, d) α = 3, e) α = 6. The depth of the cutting plane varies along the z-direction.

The contours, which are not directly involved in the closed contours show little resemblance to the layers of group 2 defined in cross-sections perpendicular to the shear direction (see chapter 2). We, therefore, do not employ the same layer classification as defined earlier for cross-section perpendicular to the shear direction. For $\alpha = -3$ (Figure 2b) closed contours are visible for all cross-sections. One cross-section even exhibits a 'double-eye'. Also for horizontal cross-sections ($\alpha = 0$, Figure 2c) closed contours are visible in all cross sections. The individual shapes of the closed contours differ significantly from the approximately elliptical shapes that we observed in cross-section perpendicular to the shear direction. For $\alpha = 3$ (Figure 2d) and $\alpha = 6$ (Figure 2e), the patterns are dominated by 'folded' layers. Only the cross-section cutting directly through the cone show closed contours.

5.4. Conclusion

Cross-sections that are approximately parallel to the shear plane show a variety of patterns. If the cross-section cuts through the cone of the fold, several closed contours nested in each other can be observed, which are similar in appearance to patterns in cross-section perpendicular to the shear direction. In such cross-sections, the shear sense could be misinterpreted by 90 degrees. The cross-section needs to cut the fold through the cone to produce patterns that can be linked to sheath folds. Cross-sections cutting through the sheath fold closer to its center show patterns dominated by 'folded' layers. Such cross-section cannot be easily linked to sheath folds.

5.5. References

Alsop, G. I., and Carreras, J., 2007, The structural evolution of sheath folds: A case study from Cap de Creus: Journal of Structural Geology, v. 29, no. 12, p. 1915-1930.

Exner, U., and Dabrowski, M., 2010, Monoclinic and triclinic 3D flanking structures around elliptical cracks: Journal of Structural Geology, v. 32, no. 12, p. 2009-2021.

Passchier, C. W., 2001, Flanking structures: Journal of Structural Geology, v. 23, no. 6-7, p. 951-962.

6. Overall conclusions

The previous four chapters showed results obtained with an analytical and experimental method. With both methods, we investigated the formation of sheath folds around weak inclusions acting as slip surfaces. The findings of these chapters and, therefore, of this thesis can be summarized in the following points:

- Sheath folds form at the tips of the deformed inclusions both in the analytical and experimental models (Figure 1).
- Inhomogeneous far-field strain is not necessary to form sheath folds.
- Cross-sections perpendicular to the shear direction in the y-z plane show three different layer structure types. 1) Undeformed or only slightly deformed layers away from the inclusion, 2) Omega (Ω) shaped layers, and 3) closed contours forming eye-patterns.
- The distribution and occurrence of the layer types is dependent on the cross-section location.

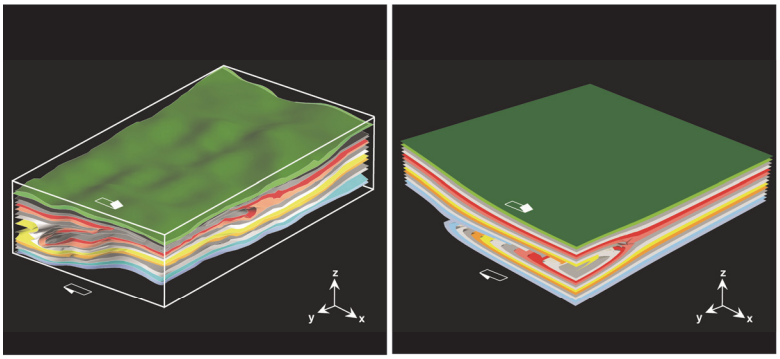

Figure 1: Left: Three-dimensional reconstruction (gOcad) of a sheath fold produced with an experiment at $\gamma = 6$, $\theta = 90°$, a/b = 2.67, and a viscosity ratio of 20. The sheath fold dips

downwards into the matrix. The white arrows indicate the shear direction. Right: Three-dimensional visualization of an analytically modeled sheath fold at $\gamma = 6$, $\theta = 90°$, $a/b = 2.67$, and a viscosity ratio of 1.

- Cross-sections parallel to the shear direction in the x-z plane show structures that are similar to flanking folds.
- Cross-sections parallel or with a small angle to the shear plane reveal a big variety of structures of which some exhibit closed contours.
- Sheath folds develop irrespectively of the slip surface orientation and shape. Both parameters have, however, an impact on the actual shape and size of the resulting fold.
- The layer thickness to inclusion height ratio plays a major role on the visibility of the sheath folds.
- Sheath folds develop in a mechanically layered matrix where the viscosity ratio between the layers is up to 20. For a viscosity ratio of 50, strongly deformed layers can be observed but no eye-structures are clearly visible.
- The viscosity ratio in the matrix has an influence on the fold length, dip, and opening angle. This can only be detected in three dimensions, while two-dimensional cross-sections strongly resemble each other.
- The shape of the outermost closed contour forming the eye-structure is dependent on the inclusion orientation, initial inclusion shape, strain, and cross-section location.
- The distribution of the location of the center of the eye-pattern as a function of the cross-section location is almost strain independent as well as almost independent on the initial settings of the inclusion. The center moves within one fold from a position in the lower half of the eye-pattern to the upper half, which results in an apparent thickening/thinning of the layers in the cross-sections.
- The layer thickness variation in eye-structures cannot be used to determine the shear sense in shear zones.
- The ratio of the aspect ratio of the innermost and outermost closed contour is dependent on the orientation and shape of the inclusion. Values above and

below 1 can be obtained in simple shear, questioning eye-pattern shapes as criterion for the bulk strain regime.

- There is no systematic and identifiable difference in eye-patterns depending on the inclusion settings, strain, cross-section location, or viscosity ratio in the matrix.
- Both, the analytical and experimental models capture the first order observations from nature such as the layer shapes and distribution in cross-sections (Figure 2).
- Double-eye-folds can be produced in a single deformation step in the analytical and experimental models (Figure 2).

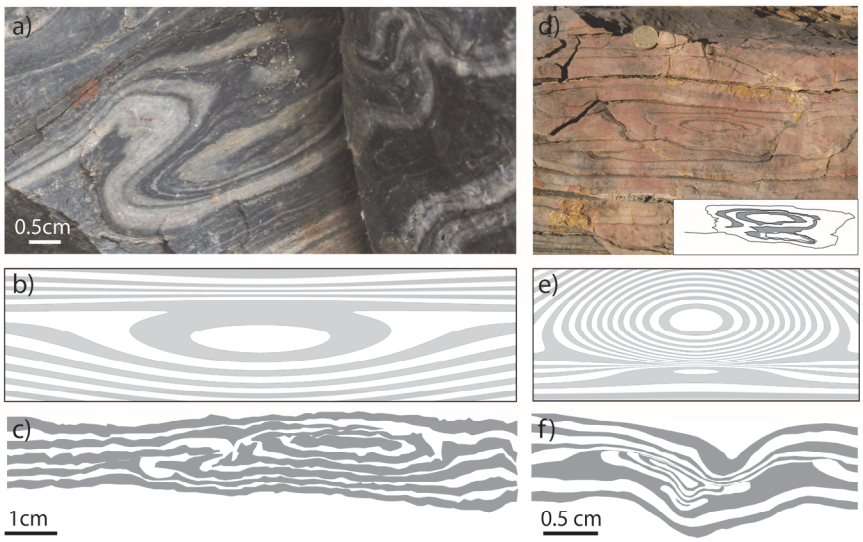

Figure 2: a) Sheath fold from Cap de Creus, Spain. b) Cross-section from the analytical model, $\gamma = 10$, $\theta = 135°$, a/b = 1, section at 12 units. c) Result from an experiment, $\gamma = 6$, $\theta = 90°$, a/b = 2.67, viscosity ratio = 20, cut at 4.5 cm from the model center. d) Double-eye sheath fold from Goantagab, Namibia. e) Cross-section from the analytical model, $\gamma = 10$, $\theta = 135°$, a/b = 1, cut at 8 units. f) Result from an experiment, $\gamma = 6$, $\theta = 90°$, a/b = 2.67, viscosity ratio = 1, cut at 5 cm.

According to these findings eye-pattern in sheath fold cross-sections show very similar features independent of the initial slip surface aspect ratio and

orientation, strain magnitude, cross-section location, or viscosity ratio in the matrix. Linking two-dimensional sheath fold outcrops to specific initial conditions is, therefore, not possible. Eye-patterns alone cannot be used as strain gauge, viscosity ratio measure, bulk strain indicator, or shear sense indicator. Also in three-dimensional outcrops of sheath folds, correlations between fold shapes and sizes to initial conditions are difficult. Even though the folds show differences in shape and size, the resulting structures are not unique. In addition, three-dimensional outcrops of sheath folds are rather rare.

The combination of an analytical model with experiments allowed for testing a large parameter space, as the two models are complementary. Both methods, however, produce very similar results for the same initial conditions. The methods, therefore, confirm each other's validity.

The findings in this thesis do not promote the usage of sheath folds as any kind of kinematic or mechanical indicator, however, there is still a long way to go until we understand how these peculiar structures form and behave in nature. The presented studies only investigated sheath folds in simple shear. So far, we did not study the effect of a pure shear component on the formation of the folds. To discard sheath folds entirely as bulk strain type indicators a systematic study of the influence of a pure shear component on the fold shape would be necessary. For a better estimate on the slip surface size, which is needed to produce sheath folds, especially in a mechanically layered matrix, thin, passive layers would have to be implemented in thick layers. This would allow observing whether a sheath fold can develop within one layer that is bounded by two layers of different viscosities. Both methods used in this thesis showed that sheath folds develop readily from weak inclusions promoting them as triggering objects. Ultimately, natural examples of such weak inclusions leading to the formation of sheath folds need to be identified to support the proposed formation mechanism.

Appendix A: PhD activities

6.1. Publications

6.1.1. Presented in this thesis

Reber J.E., Dabrowski M., Schmid D. W., 2012, Sheath fold formation around slip surfaces, *Terra Nova*.

Reber J.E., Galland O., Cobbold P. R., Le Carlier de Veslud, 2012, Experimental study of sheath fold development around a slip surface in a mechanically layered matrix, *Tectonophysics*, accepted (revisions not included).

Reber J.E., Dabrowski M., Galland O., Schmid D. W., 2012, Analytical modeling of the morphology and internal structure of sheath folds in simple shear, for submission to *Journal of Structural Geology*.

6.1.2. Other publications

Reber J.E., Schmalholz S. M., Burg J.-P., 2010, Stress orientation and fracturing during three-dimensional buckling: Numerical simulation and application to chocolate-tablet structures in folded turbidites, SW Portugal, *Tectonophysics*, 493(1-2), 187-195.

6.2. Conference Contributions

Geomod, Lausanne, 2012

Reber J.E., Galland O., Dabrowski M., Schmid D.W., Cobbold P.R., Sheath fold formation around slip surfaces in simple shear: An analytical and experimental study (Poster).

EGU Assembly, Vienna, Austria 2012

Reber J.E., Galland O., Dabrowski M., Schmid D.W., Cobbold P.R., A combined analytical and experimental study on the formation of sheath folds (Talk).

Reber J.E., Galland O., Dabrowski M., Schmid D.W., Cobbold P.R., On the usefulness of sheath folds as kinematic indicators (Poster).

25. Kongsberg seminar, Norway 2012

Reber J.E., Galland O., Dabrowski M., Schmid D.W., Cobbold P.R., Formation of sheath folds around slip surfaces: An analytical and experimental study (Poster).

AGU Fall meeting, San Francisco, USA 2011

Reber J.E., Galland O., Dabrowski M., Cobbold P.R., Schmid D.W., Formation of sheath folds around a crack: An analytical and experimental study (Poster).

Penrose Conference, Deformation localization in rock: New advances, Cap de Creus, Spain 2011

Reber J.E., Galland O., Dabrowski M., Cobbold P.R., Schmid D.W., Cracks as sheath fold initiators: Results of analytical and analogue modeling (Talk).

Geomod, Lisbon, Portugal 2010

Reber J.E., Dabrowski M., Schmid D.W., Sheath folds as late stage flanking structures: Analytical models and field observations (Poster).

Reber J.E., Schmalholz S.M., Burg J.-P., Stress evolution and fracturing during folding: 2D and 3D numerical simulations and application to chocolate-tablet structures in folded turbidites, SW Portugal (Poster).

EGU Assembly, Vienna, Austria 2010

Reber J.E., Dabrowski M., Schmid D.W., Are sheath folds late stage flanking structures? (Poster).

Nordic Winter Meeting, Oslo, Norway, 2010

Reber J.E., Schmalholz S.M., Evolution of stress and strain during 3D folding: Application to orthogonal fracture systems in folded turbidites, SW Portugal (Poster).

6.3. Courses

GEO9051SP	DEM simulations in geosciences using ESYS particle software (5 Credit points)
GEO9630	Geodynamics (10 Credit points)
FYS-GEO9510	Introduction to mechanical geomodelling (10 Credit points)
MNSE9100	Science, Ethics and Society (5 Credit Points)
Svalex	Petroleum geological excursion to Svalbard